Accuracy of turbulent flux measurements through the use of high frequency data by eddy covariance tower: the case study of Landriano (PV), Italy

Daniele Masseroni[1], Giulia Ercolani[2], Chiara Corbari[2], Marco Mancini[2]*

Abstract: *High frequency data measured by eddy covariance stations can be used for different applications, especially to obtain reliable turbulent flux estimations and to find the reason for possible errors into flux measurements. Generally, the quality of flux measurements is correlated with atmospheric turbulent characteristics and evaluated through the use of stationary or well-developed turbulence tests. However, a quantitative analysis of the error connected with each turbulent flux is not yet present in literature. In this work, starting from high frequency data of the three wind components and scalar passives, spectral analysis is used to quantify relative errors for each half-hourly flux of latent and sensible heat, momentum and carbon dioxide. The experimental dataset was obtained by a micrometeorological station located over a maize field at Landriano (PV) in Padana plain. Two different experimental time period are considered: one when the vegetation height is about 2.80 meters and second after harvesting time. The results have mainly shown a sinusoidal trend of the errors characterized by minimum peaks during daytimes, while in nighttime the measurements can be affected by imprecisions that could reach values up to 65-70%.*
Keywords: *eddy covariance, turbulent fluxes, high frequency, cross spectra, footprint.*

Riassunto: *Le misurazioni eddy covariance ad alta frequenza possono essere utilizzate per molteplici applicazioni, specialmente per la stima accurata dei flussi turbolenti e la valutazione degli errori di misura ad essi connessi. Generalmente la qualità dei flussi di massa e di energia misurati dalle stazioni eddy covariance è correlata alle caratteristiche della turbolenza atmosferica ed è valutata principalmente attraverso i test di stazionarietà e di turbolenza sviluppata. Tuttavia la stima quantitativa degli errori connessi a ciascun flusso turbolento non è ancora presente in letteratura. In questo lavoro, partendo da dati acquisiti ad alta frequenza, l'analisi spettrale è stata utilizzata per calcolare l'errore relativo connesso a ciascun valore di flusso stimato alla mezz'ora. I dati sperimentali sono stati acquisiti da una stazione micrometeorlogica posizionata all'interno di un campo coltivato a mais nel comune di Landriano (PV) in Pianura Padana. Due differenti set temporali di dati sono stati analizzati: uno quando la vegetazione è quasi al massimo del suo sviluppo fenologico e pari a 2.8 metri e l'altro dopo la mietitura. I risultati hanno mostrato un trend oscillatorio degli errori sui flussi misurati, caratterizzato da minimi relativi durante le ore diurne e massimi, che possono arrivare fino al 65-70%, durante le ore notturne.*
Parole chiave: *eddy covariance, flussi turbolenti, alta frequenza, cross spectro, footprint.*

1. INTRODUCTION

Energy and mass fluxes developed in SVAT (Soil-Vegetation-ATmosphere) systems are important for a wide range of applications at different spatial and temporal scales: from flood simulation at basin scale to water management in agricultural areas. Reliability of eddy covariance measurements has to be studied before using them in hydrological simulations (Aubinet *et al.*, 2000).

Eddy covariance stations measure turbulent fluxes of sensible and latent heat, water, carbon dioxide and momentum at agricultural field-scale, having the main objective to estimate the correct water requirement for a crop. The main instruments, which give the name to the eddy covariance technique, are gas analyzer and tridimensional sonic anemometer. They measure turbulent fluxes into surface layer (Stull, 1988), thanks to the covariance between vertical wind velocity and concentration of a scalar passive (for example: air/water, temperature or carbon dioxide).

Flux estimations are obtained through complex series of steps starting from raw data acquired with high frequencies of about 10-20 Hz. The quality of these measurements is mainly influenced by problems of sensor configuration, place of the tower and stability of the atmosphere (Foken and Wichura, 1996; Fuehrer and Friehe, 2002). Example of necessary details and considerations in

* Corresponding author: daniele.masseroni@unimi.it
[1] Dipartimento di Scienze Agrarie e Ambientali – Produzione, Territorio e Agroenergia, Università degli Studi di Milano, Italy.
[2] Dipartimento di Ingegneria Civile e Ambientale, Politecnico di Milano, Italy.
Received 31 January 2013, accepted 2 May 2013.

a typical eddy covariance system are shown in a series of papers (Shuttleworth *et al.*, 1982, Shuttleworth *et al.*, 1988; Shuttleworth, 1988).

Many efforts to obtain reliable flux measurements have been done from the birth of this micrometeorological method (Foken, 2008). Lee *et al.* (2004) formulate recommendations related to the eddy covariance technique for estimating turbulent mass and energy exchange, and give a comprehensive overview on the current state of the art regarding micrometeorological issues and methods.

In recent decades, many software implemented by different universities in the world, can be found in literature (TK3, EdiRe, EddySoft, Alteddy, EddyPro) with the main objective to standardize the correction procedure of eddy covariance measurements (Ueyama *et al.*, 2012). These softwares have been widely validated and they are all based on five fundamental points:

1) Measured data are opportunely selected in function of quality tools;
2) Data are calibrated or corrected if necessary;
3) Data are aggregated in statistic tools as mean, variance or covariance;
4) Data are converted in averaged fluxes;
5) Reliability of fluxes is evaluated.

Generally, stationary or well-developed turbulence tests (Foken and Wichura, 1996) are used to evaluate flux reliabilities in function of the turbulent characteristics of the surface layer, discarding the data if the tests are not verified. These tests do not give direct information about the quality of fluxes but, in order to achieve a good dataset quality, they help to verify if theoretical assumptions, which govern the eddy covariance technique, are not guarantee (Foken, 2008).

The main objective of this work is to find a method which permits to quantify an error associated with each turbulent flux, so that, for operative applications, the operator can choose a threshold (which is consistent with the objective of his work) beyond which the data can be discarded. Frequency analysis of spectra and cross-spectra have been used to quantify the amount of each flux error. The large amount of data collected by various investigators show clear indication that spectra of wind velocity, temperature and vapor or carbon dioxide concentrations, obey to the similarity theory (Foken, 2008) over a range of frequencies called inertial sub range (Kaimal *et al.*, 1972). Typical spectra shapes for different turbulent variables can be found in Kaimal *et al.* (1972), Baldocchi and Mayers (1988) and Baldocchi *et al.* (1988). Theoretical treatments conclude that the slope of the velocity and temperature spectrum in the inertial sub-range and in log-log space is $-5/3$, while the cross spectrum for momentum, latent, sensible heat and carbon dioxide fluxes becomes $-7/3$ (Wyngaard and Cote, 1972). Comparing theoretical and experimental spectrum slopes, it will be possible to calculate the relative error for each half-hour turbulent flux, as shown in this work.

In an eddy covariance station, besides the high frequency acquisition of the turbulent component of vertical wind speed, air temperature or relative humidity, is required the study of flux representativeness which are referable to an area surrounding the station. In fact, the relation between the intensity of source upwind of a sensor and the value of the signal registered by this sensor can be described quantitatively with the help of the footprint function (Schmid, 2002; Kormann and Meixner, 2001; Kljun *et al.*, 2002; Hsieh *et al.*, 2000). Using high frequency data of the wind velocity components, Masseroni *et al.* (2012) show that there is a relationship between the representative source area for eddy covariance measurements, and the large eddies responsible for the transport of turbulent kinetic energy. Comparing integral length of the large eddies, obtained from autocorrelation function of the high frequency data, with the results of the Hsieh *et al.* (2000) analytical footprint model, the good accuracy of the Masseroni *et al.* (2012) method, which estimates the turbulent flux footprint, is also shown. The results have been subsequently overlapped on a Google map image of the field in order to understand what are the parts of the field which contribute to the flux measurements.

2. DATA COLLECTION AND INSTRUMENTS

Experimental data have been obtained by a micrometeorological station mainly used to measure evapotranspiration fluxes in a maize field at Landriano (PV) in Po Valley (45.19 N, 9.16 E, 87 m a.s.l). The field is about 10 hectare large and it has a polygonal geometric structure surrounded by row plant on three site. Neighbor fields were maize cultivated and the plant phenological grows were the same. The experimental campaigns cover two different time period over 2011 growing season: one from 22 July to 4 August (Case A) when the vegetation height is 2.80 meters and the other one from 14 September to 23 September (Case B) after harvesting time.

The station has been equipped with C1 Class

	Case A		Case B	
Atmospheric conditions	**Number of data**	**Percentage of data (%)**	**Number of data**	**Percentage of data (%)**
Total data set	614	100.00	300	100.00
Unstable	286	46.57	176	58.67
Neutral	162	26.38	25	8.33
Stable	166	27.04	99	33.00

Tab. 1 - Number of data (mean value over an averaging time of 30 minutes) for each atmospheric stability class.
Tab. 1 - Numero di dati (valori mediati con passo temporale di 30 minuti) suddivisi per ciascuna classe di stabilità atmosferica.

different devices for the measure of various meteorological parameters, from air temperature to soil moisture. However, for the analysis described in this work, only one three dimensional sonic anemometer (Young 81000 by Campbell Scientific) and one gas analyzer (LICOR 7500 by LI-COR) have been used. The former provide for the three wind components and sonic temperature measurements, while the latter provide for the water vapor and carbon dioxide air concentrations. Both instruments have been located at the top of the tower at 5 meters high and both are set to 10 Hz acquisition frequency. The data have been stored in a Compact flesh of 2Gb connected with a Data Logger CR5000 (Campbell Scientific) and subsequently subdivided in 30 minutes aggregation time groups.
The data have been corrected applying the whole range of correction procedures described in Aubinet *et al.* (2000). Axis rotation for tilt correction, spike removal, time lag compensation and detrending, which represent the preliminary processes to prepare the dataset for covariance calculation, have been firstly computed. These corrections have been applied using an automatic procedure PEC (Polimi Eddy Covariance) implemented by Politecnico of Milano (Corbari *et al.*, 2012).
In order to estimate the relative error for each half-hourly flux, the whole dataset in Case A and B has been used, while for the footprint analysis only data in unstable conditions of the atmosphere have been implemented. To define the different stability conditions of the atmosphere, the stability parameter described by Hsieh *et al.* (2000) has been used and in Tab. 1 the data subdivision in different stability classes is shown. The total number of data, over an averaging period of 30 minutes, is about 600 and 300 for the Case A and B respectively. In both cases about 50% of the eddy covariance measurements belong to the unstable conditions of the atmosphere while only 28% is in stable conditions. The prevalent wind directions, during the experimental campaigns, is West and about 40% of the total datasets come from North-West to South-West sectors.

3. METHODOLOGY

3.1. Spectral analysis

Spectral analysis is a statistic tool that can be employed to probe further into the workings of turbulence. By decomposing a series of measurements into frequency or wave number components, it is possible to discover how eddies of different time and space scales contribute to the overall turbulence state (Stull, 1988).
Spectral densities have been directly obtained from Fourier coefficients of a series of measurements and they have been calculated using FFT algorithm (Bendat and Piersol, 1986). According to Kolmogorov's law (Garrat, 1993), for the inertial subrange, the cross spectrum for latent and sensible heat, momentum and carbon dioxide is proportional to the frequency elevated to -7/3. Experimental cross spectra could have an exponent of scale which is different by the theoretical one, so that the relative error between these two exponents represents the error associated with each turbulent flux. Generally, the cross spectrums are calculated starting from a couple of variables (e.g. vertical wind velocity and temperature, vertical wind velocity and water vapor) therefore, the cross spectrum is referred to the covariance of these two components, as widely explained by Wygnard and Cotè (1972). Since turbulent fluxes are calculated starting from the covariance between vertical wind velocity and concentration of a scalar passive (Barr *et al.*, 2006), in this study the relative error for each covariance typologies is supposed to be equal to the error associated with the corresponding flux.

3.2. Footprint analysis

The turbulence scales of the instantaneous wind speed are the measure of the representative dimensions of the vortices induced by the turbulence inside the mean stream of the flow (Teleman *et al.*, 2008). The determination of the turbulence scale starts computing the autocorrelation function for all fluctuation components (longitudinal, transversal, vertical) of the wind speed. According to the Taylor's hypothesis of the "frozen turbulence" (Foken, 2008) and supposing that the turbulence is homogeneous and isotropy, the integral length along the wind direction is computed. Subsequently, the integral length, has been compared with the footprint dimension obtained by the Hsieh *et al.* (2000) model during unstable conditions of the atmosphere. Stable conditions of the atmosphere have been not taken into account because, for the proprieties of footprint model, fetch dimension tends to become larger than the size of the field. Hsieh *et al.* (2000) analytical footprint model has been chosen because it is widely used in literature to study the representativeness of turbulent flux measurements by eddy covariance towers. It can be applied on the whole range of stability conditions of the atmosphere and its structural algorithm is computationally easy to implement. In this paragraph mathematician computations and procedures are not deeply shown but they are widely described in Masseroni *et al.* (2012) work.

4. RESULTS AND DISCUSSIONS

4.1. Case A

Using high frequency data of wind velocity components, sonic temperature and scalar passives, the cross spectra for the principal turbulent fluxes (momentum, latent heat, sensible heat and carbon dioxide) have been calculated. In Fig. 1 an example of 30 minutes cross spectrum of the covariance between turbulent components of vertical wind and sonic temperature is shown and the black line represents the theoretical slope.

Analyzing the slope of the experimental cross spectrum into the inertial sub range, and comparing it with the theoretical -7/3 slope, the relative error in percentage terms is computed, and the results in functions of time are shown in Fig. 2.

The data shown in Fig. 2 have been filtered with a moving average of period ten. The five covariances shown in Fig. 2, have a minimum error of about 40%. This is probably due to impossibility of respecting the isotropic Kolmogorv's hypothesis. In

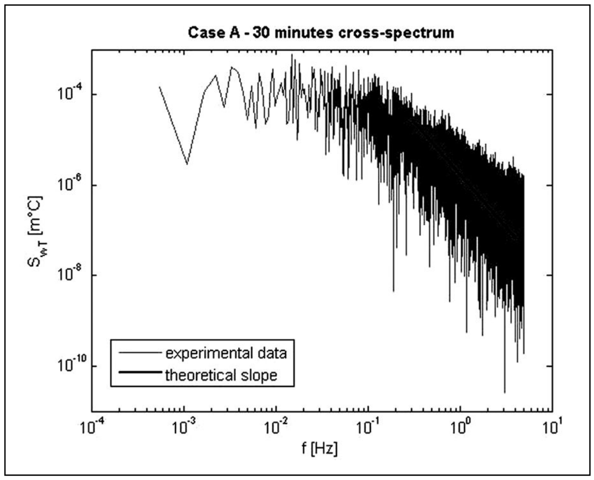

Fig. 1 - Cross spectrum of the covariance between vertical wind component and sonic temperature. The black line represents the theoretical slope.

Fig. 1 - Cross spectrum della covarianza tra la componente verticale della velocità del vento e la temperature sonica. La linea nera rappresenta la pendenza teorica dello spettro nell'inertial sub-range.

fact the eddies, in real conditions, are not perfectly isotropic because their shape is strongly influenced by the convective force, the shear stress, the wake production energy and the energy cascade processes (Griffith *et al.*, 1956, Leaviti, 1975). Moreover, a residual instrumental error connected with the measurement proprieties (Ueyama *et al.*, 2012) precludes the possibility to reach perfect measurements without any errors.

The error time series is characterized by a periodic form with a minimum in correspondence of daytime while during the night the relative error can also be about 65-70%. This is probably due to stable conditions of the atmosphere, low turbulence and advection flows which appear to be localized typically during the nighttime. The turbulent fluxes measured in this period show a bad quality and they can be generally considered incorrect.

4.2. Case B

In Fig. 3, for the Case B, the relative errors in function of time are shown. The original curve has been filtered with a moving average of period twenty. Also in this case, the minimum error is about 40% . All the relative errors, from momentum to carbon dioxide flux, have the same periodic shape. The crest is shown in the nighttime while the gorge in daytime. It is important to underline that some nighttime periods the errors could decrese at about 40-50% as a consequence of particular atmospheric conditions. In fact, during the night time, generally,

the stable conditions of the atmosphere are dominant, but if the wind velocity is intense, the shear stress constitutes the turbulent forcing which allows the eddy covariance station to measure correctly the energy fluxes.
As shown in Fig. 2 and 3 also if the experimental campaigns are carried out in two different time periods, with and without the presence of vegetation, the results are not particularly influenced by the plants and the relative errors, in both cases, have a similar quantitative behavior.

4.3. Footprint comparisons

To compare integral length and footprint dimension, the wind direction for each data has been calculated. The wind directions have been subdivided into 72 classes, each of 5° large. In function of these wind direction classes, fetch and integral length have been organized and a mean value of footprint and integral length has been calculated.
In Fig. 4, comparison between fetch (dot line) and integral length (solid line), in Case A and B, are shown. The results have been overlapped to a Google map image of the field and opportunely scaled with the field dimension and centered with station position. In Case A the footprint dimension is approximately less than 50 m in respect to case B. In fact, as show in Hsieh *et al.* (2000), footprint is directly proportional to the measurement height. When the field is covered by vegetation the measurement height has to be subtracted for a displacement factor (Foken, 2008) which reduces the footprint length. In both cases the representative area for turbulent fluxes is included into the field edges. Integral and footprint length have a quite similar shape, which is mainly imposed by stability condition of the atmosphere, wind speed

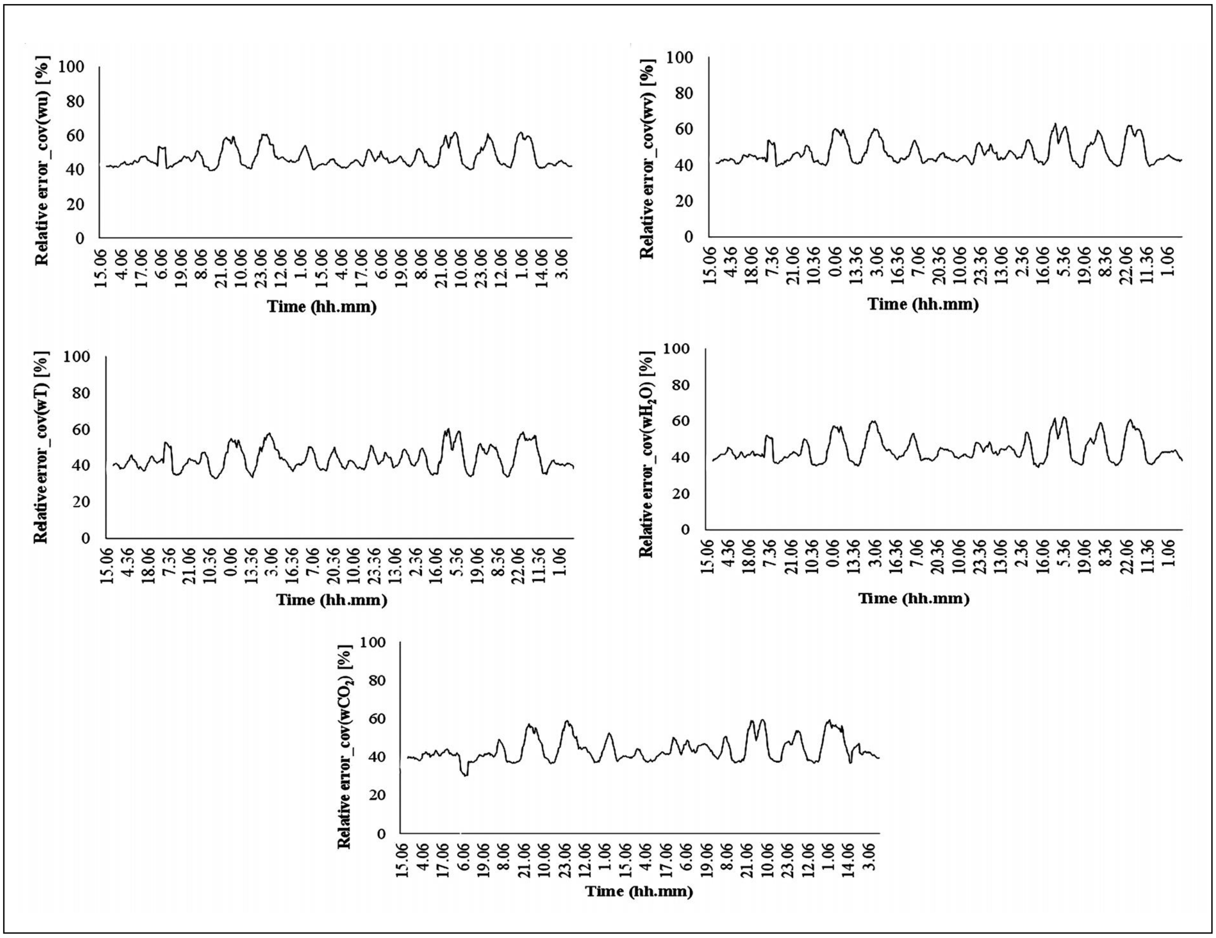

Fig. 2 - Relative error trend in function of time for the turbulent fluxes of momentum (cov(wu) and cov(wv)), sensible heat (cov(wT)), latent heat (cov(wH_2O)) and carbon dioxide (cov(CO_2)) for the Case A.
Fig. 2 - Trend dell'errore relativo in funzione del tempo per i flussi di quantità di moto (cov(wu) e cov(wv)), calore sensibile (cov(wT)), calore latente (cov(wH_2O)) e anidride carbonica (cov(CO_2)). Caso A.

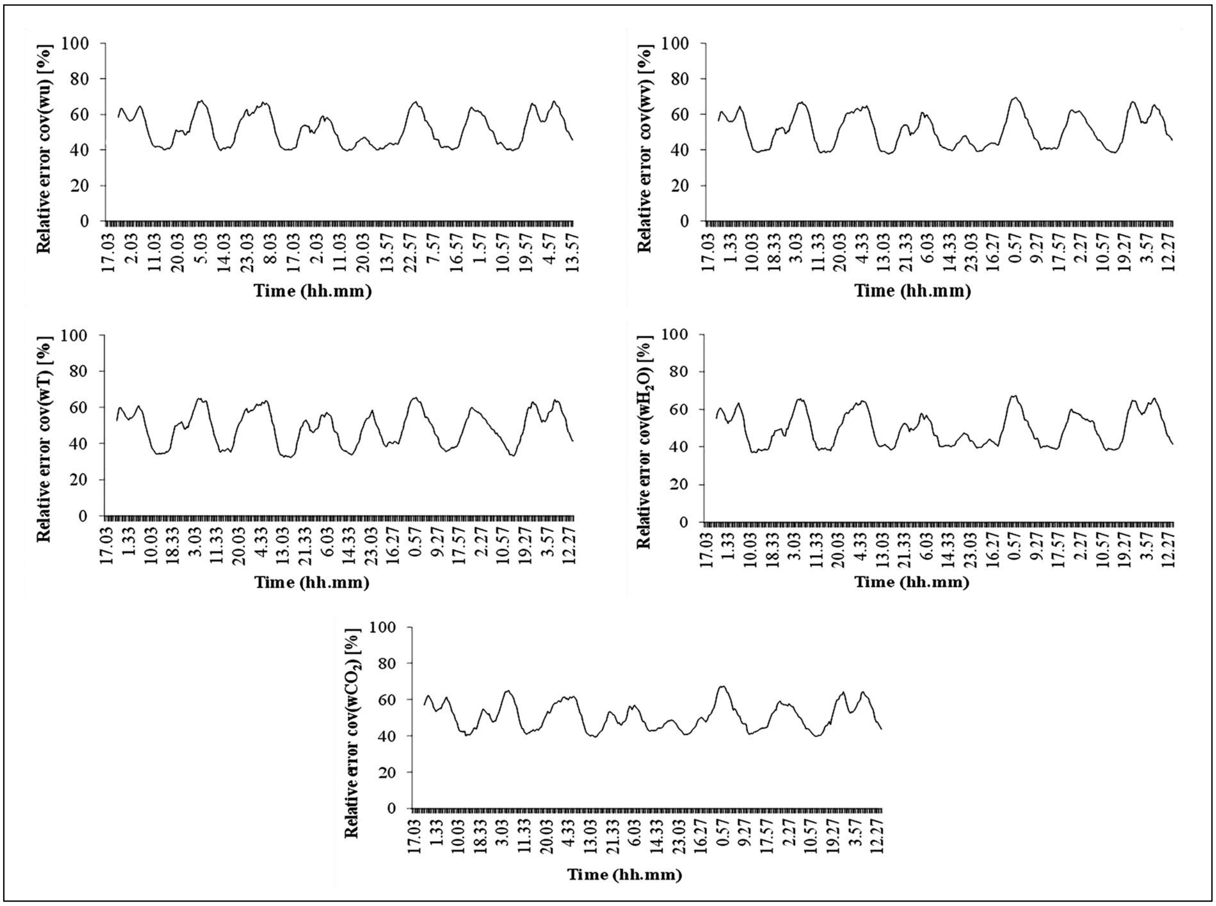

Fig. 3 - Relative error evolutions in function of time for the turbulent fluxes of momentum (cov(wu) and cov(wv)), sensible heat (cov(wT)), latent heat (cov(wH_2O)) and carbon dioxide (cov(CO_2)) for the Case B.

Fig. 3 - Trend dell'errore relativo in funzione del tempo per i flussi di quantità di moto (cov(wu) e cov(wv)), calore sensibile (cov(wT)), calore latente (cov(wH_2O)) e anidride carbonica (cov(CO_2)). Caso B.

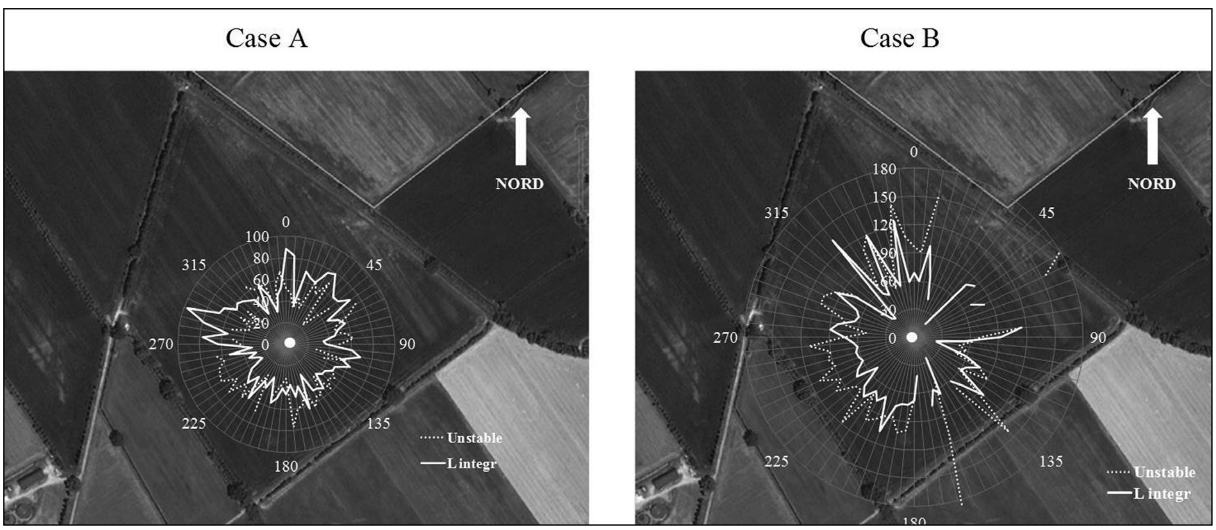

Fig. 4 - Footprint and integral length dimensions shown over Google map field image. The white dot represents the position of the eddy covariance tower.

Fig. 4 - Footprint e lunghezza integrale sovrapposte ad un immagine di Google del campo sperimentale di Landriano. Il punto centrale rappresenta la posizione della stazione eddy covariance.

and directions, with a relative error between them of about 13% in the Case A and -17% in the Case B. A negative error means that more or less, over total dataset, the footprint is larger than integral length.

5. RELATIVE ERRORS FOR DIFFERENT AVERAGING PERIODS

Generally, turbulent fluxes for agricultural applications are averaged over a time period of 30 minutes. However, it is very important to understand how, starting from high frequency acquisitions, relative error for each flux changes over different averaging periods (from 1 to 180 minutes).

For each averaging period, mean value of relative error between theoretical and experimental spectrum slope has been calculated, and in Fig. 5 the results are shown. In both cases relative error tends to decrease when the averaging period come from 1 to 180 minutes. In fact, in accordance with Taylor's hypothesis (Stull, 1988), when averaging period is small, large eddies could not be taking into account during mathematical approaches for the statistical calculations (determination of the variances and covariances).

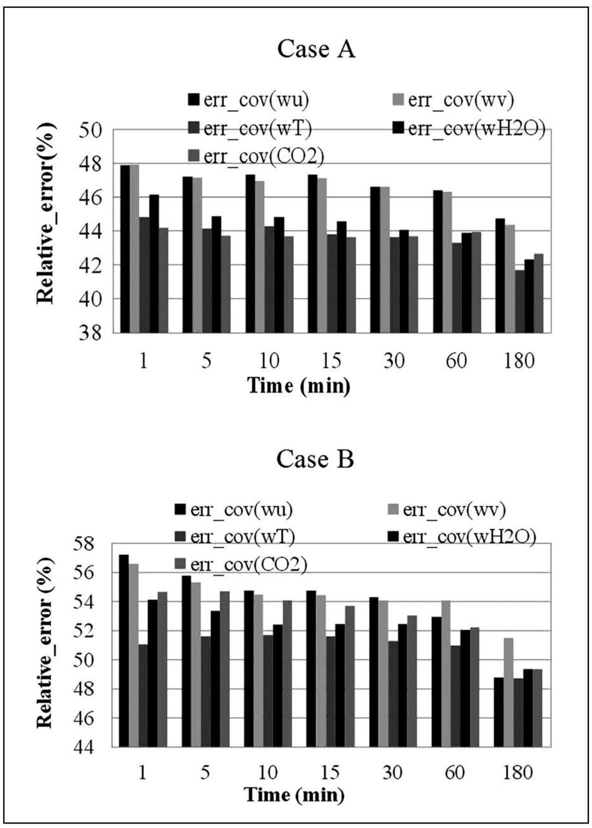

Fig. 5 - Relative errors for different averaging periods.
Fig. 5 - Errori relative per differenti tempi di mediazione.

In bare soil (Case B) the relative errors are greater than Case A. This is probably due to the absence of the surface homogeneity after the harvesting time when, on the field, waste products of the plants and bare soil are contemporaneously present on the surface. Moreover, in non-particular convective situations, turbulent flux representative source areas could be beyond the field edge, so that measurement errors tend to increase drastically.

6. CONCLUSIONS

In this work, turbulent fluxes of sensible and latent heat, momentum and carbon dioxide, have been computed using a frequency method starting from high frequency measurements of wind speeds, sonic temperature and scalar passives. Through cross spectrum analysis, an innovative method to measure the quality of fluxes has been shown. Flux relative errors cover a wide percentage range which come from 40% to about 70%. Good quality of data is shown during daytime while in nighttime error peaks reach values up to 70%. Stability conditions of the atmosphere, advection situations and low turbulence play a substantial role in degradation of quality fluxes. Generally, in convective situations, flux footprint is inside the field edges while in stable conditions, and in some cases of bare soil, representative source area for turbulent fluxes exceeds the field edges and measurement reliabilities could get worse.

ACKNOWLEDGEMENTS

This work was funded in the framework of the ACQWA EU/FP7 project (grant number 212250) “Assessing Climate impacts on the Quantity and quality of WAter” , the framework of the ACCA project funded by Regione Lombardia “Misura e modellazione matematica dei flussi di ACqua e CArbonio negli agro-ecosistemi a mais” and PREGI (Previsione meteo idrologica per la gestione irrigua) founded by Regione Lombardia. The authors thank the University of Milan – DiSAA for the collaboration given in managing Landriano eddy covariance station.

REFERENCES

Aubinet M., Grelle A., Ibrom A., *et al.* (2000). Estimates of the annual net carbon and water exchange of forests: the euroflux methodology. *Advanced in Ecological Research* , 30: 113-175.

Baldocchi D., and Meyers T. (1988). A spectral and lag-correlation analysis of turbolance in a deciduous forest canopy. *Boundary Layer Meteorology* , 45,31-58.

Baldocchi D., Hicks B., and Meyers T. (1988). Measuring biosphere-atmosphere exchanges of biologically related gases with micrometeorological methods. *Ecology*, 69, 1331-1340.

Barr A., Morgenstern K., Black T., McCaughey J., and Nesic Z. (2006). Surface energy balance closure by the eddy-covariance method above three boreal forest stands and implications for the measurement of CO_2 flux. *Agricultural and Forest Meteorology*, 140, 322-337.

Bendat J., and Piersol A. (1986). Decomposition of wave forces into linear and nonlinear components. *Journal of sound and Vibration*, 106, 391.

Corbari C., Masseroni D., and Mancini M. (2012). Effetto delle correzioni dei dati misurati da stazioni eddy covariance sulla stima dei flussi evapotraspirativi. *Italian Journal of Agrometeorology*, 1, 35-51.

Foken T. (2008). *Micrometeorology.* Berlin: Springer, pp. 306.

Foken T. and Wichura B. (1996). Tools for quality assessment of surface-based flux measurements. *Agricultural and Forest Meteorology*, 78: 83-105.

Fuehrer P.L. and Friehe C.A. (2002) Flux correction revised. *Boundary Layer Meteorology*, 102: 415-457.

Garratt J. (1993). *The atmospheric boundary layer.* Cambridge: Cambridge university press, pp. 316.

Griffith H., Panofsky H., and Van der Hoven I. (1956). Power-spectrum analysis over large ranges of frequency. *Journal of meteorology*, 13, 279-282.

Hsieh C., Katul G., and Chi T. (2000). An approximate analytical model for footprint estimation of scalar fluxes in thermally stratified atmospheric flows. *Advanced water resource*, 23, 765-772.

Kaimal J., Wyngaard J., Izumi Y., and Cotè O. (1972). Spectral characteristics of surface-layer turbolence. *Quart. J.R. Met. Soc.*, 98, 563-589.

Kljun N., Rotach M., and Schmid H. (2002). A three-dimensional backward lagrangian footprint model for a wide range of boundary-layer stratification. *Boundary-Layer Meteorology*, 103, 205-226.

Kormann R., and Meixner F. (2001). An analytical model for non-neutral stratification. *Boundary layer meteorology*, 103, 205-224.

Leaviti E. (1975). Spectral characteristics of surface layer turbolance over the tropical ocean. *Journal of physical oceanography* , 5, 157-163.

Lee X., Massman W., and Law B. (2004*). Handbook of Micrometeorology: A Guide for Surface Flux Measurement and Analysis*. Kluwer Academic Press, Dordrecht, 250 pp.

Masseroni D., Ravazzani G., Corbari C., and Mancini M. (2012). Turbolence integral length and footprint dimension with reference to experimental data measured over maize cultivation in Po Valley, Italy. *Atmosfera*, 25, 183-198.

Schmid H. (2002). Footprint modeling for vegetation atmosphere exchange studies: a review and perspective. *Agricoltural and fores meteorology* , 113, 159-183.

Shuttleworth W. (1988). Corrections for the effect of background concentrations change and sensor drift in real time eddy correlation systems. *Boundary Layer Meteorology*, 42:167-180.

Shuttleworth W., Gash J., Lloyd C., McNeil D., Moore C., and Wallance J. (1988). An integrated micrometeorological system for evaporation measurement. *Agricultural and Forest Meteorology*, 43: 295-317.

Shuttleworth W., McNeil D., and Moore C. (1982). A switched continuous-wave sonic anemometer for measuring surface heat fluxes. *Boundary Layer Meteorology*, 23: 425-448.

Stull R. (1988). *An introduction to boundary layer meteorology.* Dordrecht, Boston, London, 666: Kluwer Academic Publisher.

Teleman E., Radu S., Axinte E., and Pescaru R. (2008). Turbolance scales simulations in atmospheric boundary layer wind tunnels. *Universitatea Tehnica, 'Gheorghe Asachi' din Iasi Tomul LIV (LVIII)*, Fasc. 2.

Ueyama M., Hirata R., Mano M., Hamotani K., Harazono Y., Hirano T., Miyata A., Takagi K., and Takahashi Y., (2012). Influences of various calculation options on heat, water and carbon fluxes determined by open- and closed –path eddy covariance methods. *Tellus B*, 64: 1-26.

Wyngaard J., and Cotè O. (1972). Cospectral similarity in the atmospheric surface layer. *Quart. J.R. Met. Soc.*, 98, 590-603.

Modelling the effects of meteorological and geographical drivers on damage from late radiation frost on apple trees in Northeast Iran

Mohammad Rahimi[1], Emanuele Eccel[2]*

Abstract: *Late frosts occurring in spring create significant bud damage and decrease yield of fruit trees, especially apples, in Northeast Iran. Assessment and risk modelling of late radiation frost damage would be useful to manage and decrease the damage. In order to model frost damage risk, 12 driving variables were selected, including meteorological (minimum temperature, temperature decrease rate, temperature increase rate, date of frost, cumulative degree days, area below zero line, and frost duration) and geographical ones (elevation, longitude, latitude, aspect, and slope). Three damaging radiative frosts were detected in the period of apple flowering time, 20 April 2003, 8 April 2005, and 28 March 2005 cases. Required meteorological data were collected from nine meteorological standard stations located in the apple cultivation area of Northeast Iran. Linear multiple regression was used to model the relationships. Each parameter was spatially interpolated and estimated according to a 5 by 5 km grid in order to extract input data for the model. The regression equation is significant at the level of 5%. This equation fulfils the aim to assess and map frost risk damages for apple production. The regression equation of observed and predicted frost damage risk obtained a correlation index of 0.92.*
Keywords: *late spring frost, minimum temperature, linear multiple regression, Iran, apple.*

Riassunto: *Nell'Iran nordorientale le gelate tardive creano significativi danni alle gemme e diminuiscono il raccolto degli alberi da frutto, specialmente sul melo. Una stima e una modellistica del rischio del danno da gelate radiative tardive può risultare utile per gestire e diminuire tale danno. Per modellizzare il rischio di danno, sono state selezionate 12 grandezze, che comprendono variabili meteorologiche (temperatura minima, tasso di diminuzione della temperatura, tasso di aumento della temperatura, data della gelata, gradi giorno cumulati, area sotto la linea dello zero, durata della gelata) e geografiche (altitudine, latitudine, longitudine, esposizione e pendenza). Sono state selezionate tre gelate radiative che hanno provocato danni nel periodo della fioritura: 20 aprile 2003, 8 aprile 2005 e 28 marzo 2005. I dati meteorologici necessari sono stati ricavati da 9 stazioni meteo convenzionali nel nordest iraniano. È stato quindi creato un modello regressivo multilineare per le relazioni agenti - danno. Le variabili usate per creare il modello sono state spazializzate e stimate secondo una griglia di 5 km x 5 km. L'equazione lineare risultante è significativa al 5%. Questa equazione soddisfa l'obiettivo di mappare quantitativamente i rischi di danno da gelo sulla coltivazione del melo. L'indice di correlazione fra dati osservati e simulati è pari a 0.92.*
Parole chiave: *gelate tardive primaverili, temperature minima, modelli lineari multiregressivi, Iran, melo.*

1. INTRODUCTION

Apple is one of the most important crops of the Khorasan Razavi province, Iran. The entire cultivated area in the province is over 16000 hectares (www.koaj.ir). There is a lot of apple farms in the region, having different dimensions, in general ranging from 1 to 5 ha. The apple variety mainly grown in Northeast of Iran is Golden Delicious.

Apple trees are well adapted to cold climates. Thanks to winter hardening, they can stand temperatures lower than -40 °C (Lindén *et al.*, 1996). In general, such temperatures are never attained where apple is grown; however, if the frost event takes place during the growing season, relatively severe frosts can cause damage, particularly during the reproductive cycle (Porteous, 1996). This adversity also affects apple production in Iran (Farajzadeh *et al.*, 2010), while for other crops in general, frost can be an adversity even in areas of the world which are more typically characterized by general warm climatic conditions, like Brasil (Avissar and Mahrer, 1988a) and Turkey (Erlat and Türkes, 2011). In the spring frost of March 2007 about 11000 hectares of fruit trees suffered damage, including 10000 hectares devoted to apple production in Northeast Iran. The amount of damage, based on declared Agriculture Organization of Khorasan Razavi province

* Corresponding author e-mail: mrahimi@sun.semnan.ac.ir
[1] Semnan University, Faculty of Desert Studies, Molavi Blvd, Saadi Sq., Semnan, Iran.
[2] Sustainable Agro-ecosystems and Bioresources Department, IASMA Research and Innovation Centre, Fondazione Edmund Mach, San Michele all'Adige, (I).
Received 28 December, accepted 30 June 2013.

(www.koaj.ir), was 1.7 Million USD. Frost damage of agricultural products depends on location, time, product type and environmental conditions. What factors determine the damage, and the contribution of each driver to the occurrence of frost, are important issues to be investigated. The damage rates depend on static features such as geographic and topographic characteristics of a region, and on dynamic features such as intensity and duration of frosts. Thus, by quantifying the effective role of single agents in the frost occurrence, the risk of damages to a specific crop in a particular geographic area could be zoned.

Many studies have reported the role of meteorological and geographical parameters on frost damage risk. For example, Bootsma (1976) studied minimum temperatures and risk of frost in the mountainous lands in Canada. He concluded that the average estimated frost dates occurring in the valley bottom were 34 days later in spring and 39 days earlier in fall than at higher elevations. Avissar and Mahrer (1988b) developed a three-dimensional model to simulate the local scale micro-climate zones near ground level during the occurrence of radiative frost nights in non-uniform lands. Effective parameters of this model included topography, vegetation, soil humidity, wind speed and direction, and air humidity. Kajfez (1987) defined a relationship between the first occurrence of early autumn frost date and elevation. Laughlin and Kalma (1988) studied minimum temperature measured over three consecutive winters in an open area. They showed that the minimum air temperature changes with height, mean wind speed at night, the total net radiation at night, and minimum temperature estimated over the hill. Therefore, it was possible to calculate frost risk with weather data, and regional and local land analysis. Zinoni *et al.* (2002) conducted a climatological and orographic study to identify areas prone to frost and determine characteristics of frost events in the period April 1987 to March 2000 for 161 meteorological stations in the Emilia-Romagna region, Italy. They determined correlations among climatic and orographic variables and defined a significant correlation between the mean minimum temperature during the frost and the relative height from valley bottom. Richards and Baumgarten (2003) showed that the spatial distribution of radiation frosts is closely associated with topographic patterns. They prepared a minimum temperature map by using GIS modelling and factors such as ground cover, slope, elevation, latitude, and distance to the sea. Madelin and Beltrando (2005) studied spring late frost risk hazard zonation in grape vineyards in France. They used a digital elevation model to create a minimum temperature distribution map in the study area based on 20 meteorological station data. Eccel *et al.* (2008), aiming at late frost spatial modelling, measured ground temperature by airborne thermal infrared images during a strong thermal inversion episode in a fruit-growing area, showing the existence of a clear geographic pattern in the distribution of minimum temperature. All of these studies highlight the role of micro-climate and geographical parameters on frost risk.

In recent years, frost studies in Iran, despite the importance and amount of damage caused by this adversity to fruit production in the country, have been somewhat limited, mostly considering just statistical occurrence and synoptic aspects. Frost was first studied in Hashemi (1977) for the late (spring) and early (autumn) frosts occurring in Iran, based on data from 17 meteorological stations. Alizadeh *et al.* (1994) studied first and last occurrences of frosts at 15 weather stations of the Khorasan province. These studies were based on single sites, and no attempt was made to obtain regional rules. All previous frost studies in Iran measured the relationship of frost intensity to the frost damage and estimated the various probabilities of occurrence in the form of statistical distributions. No investigation on the assessment of the effects of forcing agents on frost damage was undertaken till now in Iran.

The purpose of this research is the quantitative assessment of this relationship for frost risk damage on apple trees in the Northeast of Iran. This was accomplished by identifying the factors affecting frost damage and integrating them through multiple regression and GIS, providing a model for the evaluation of frost damage hazard. This could be useful for insurance and development practices, as well as for fruit growers, to protect apple trees from frost damage.

2. DATA AND METHODS

2.1 Study area

The study area is part of Khorasan Razavi province of Iran, which is located on the Mashhad plain between the two mountains of Binalud and Hezar Masjed in northeast Iran. The latitude range of the study area is from 36 to 37 degrees North and the longitude is from 58.30 to 60 degrees East (Fig. 1). The approximate area of the study region is about 13000 km^2. It includes the major cities of Mashad,

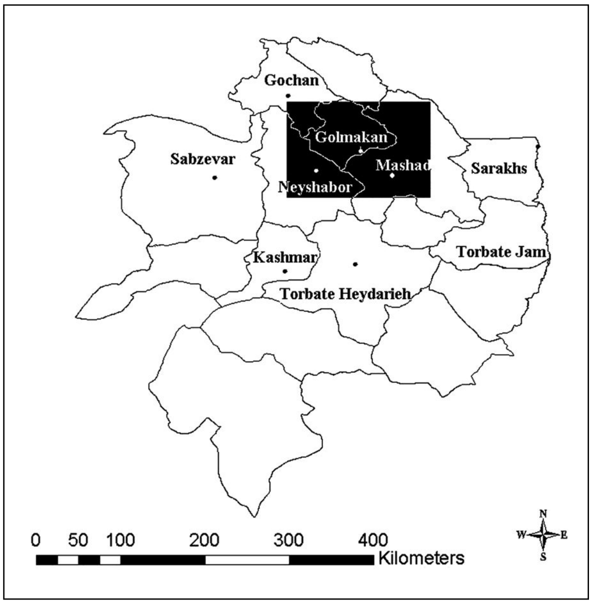

Fig. 1 - Map of Khorasan Razavi province, study area (in black), and meteorological stations (dots).
Fig. 1 - Mappa della provincia di Khorasan Razavi, area allo studio (in nero) e stazioni meteorologiche (punti).

Neyshabor, and Golmakan. This region is one of the most important places for apple production in Iran. The main variety, well adapted for the climate of this region, is Golden Delicious, like in most places in Iran.

2.2 Meteorological and geo-morphological analysis

Data from 9 synoptic stations were used in this study. Golmakan, Mashad and Neyshabor stations are located inside the study area, while the other stations are located outside. The geographical location of stations is shown in Fig. 1. Meteorological data used were minimum temperature, area below the zero line, temperature decreasing rate, temperature increasing rate, day of the year of frost occurrence, cumulative degree days with a 5°C base, and frost duration in hours.

The area below the zero line is the area between the curve of negative air temperature in a day and the zero line, in °C hour.

Temperature decreasing rate is the slope of temperature change from 21:00 to 06:00 local time in the next day (rate of temperature decrease during the nine past hours). Temperature increasing rate is the slope of trend of a temperature line from 6:00 to 15:00 local time (rate of temperature increase during 9 hours after frost). Both factors are in °C h^{-1}.

Other parameters used in modelling included altitude, latitude, longitude, slope, aspect, and frost date, expressed as day of the year (1-365) (Rahimi *et al.*, 2007).

2.3. Phenological modelling

Based on phenological observations from 1999 to 2007 at the agricultural meteorology research station of Golmkan in northeast Iran, an average initial flowering date has been observed for apple in the period 5th to 30th April. The flowering stage is critical for frost damage, because bud resistance to cold suddenly lowers in the proximity of flowering (Farajzade, 2010).

Apple trees need to satisfy chilling requirements in order to end dormancy and to start spring growth and budding. The results of Farajzadeh *et al.* (2010) were used to provide cumulative degree days. According to the mentioned study, 5 °C and 150 degree days were taken as minimum temperature threshold (Tc) and Cumulative Degree Day (CDD), respectively, for the Golden delicious variety of apple (Farajzadeh *et al.*, 2010).

2.4. Analysis of frost damages

About 12 frost events occurred in Khorasan Razavi province in 2003 and 2005 while no late frost occurred in 2004 as shown in Tab. 1. Minimum temperatures recorded at the three stations inside the study area are also shown.

Frosts can be classified into two main types: radiative and advective. In the former case, air cooling is mainly due to the heat loss toward the sky (generally clear). In this conditions air is still, and thermal inversion strongly enhanced, having as a consequence the accumulation of cold air in geographical and morphological basins, and giving rise to a moderate flow in the slope areas. In some cases, this can be lived as a "local advection" episode, although the temperature profile is stable. In the latter case, freezing is strengthened by the irruption of very cold air, advected by moderate to strong winds, originating from the movement of cold continental, polar air. In order to define and distinguish radiative from advective frosts, several factors including wind speed, temperature inversion and cloudiness were used (Davis, 1976). Determination of the temperature inversion requires air temperature data at different heights from the surface of the earth. These data can be obtained from radiosondes, whose records include vertical profiles of 5 weather elements (temperature, air pressure, humidity, wind speed and direction) and are received by the ground station every 5 minutes. These data were available from Mashhad upper

Damage occurrence	Date	Inversion	Minimum Temperature (Mashhad)	Minimum Temperature (Golmakan)	Minimum Temperature (Neyshabor)	Frost Type
frost causing no damage	19 Apr 2003	Normal	-0.6	-1	0	Advective
frost causing damage	**20 Apr 2003**	**Inversion**	**-1**	**-1.6**	**0**	**Radiative**
frost causing no damage	21 Apr 2003	Normal	-1	-0.8	0.6	Advective
frost causing no damage	26 Mar 2005	Normal	1	-1.6	0.6	Advective
frost causing no damage	27 Mar 2005	Normal	-1.4	-3	-0.8	Advective
frost causing damage	**28 Mar 2005**	**Inversion**	**-5.4**	**-4.4**	**-7.2**	**Radiative**
frost causing no damage	29 Mar 2005	Inversion	0	-0.6	-1.8	Radiative
frost causing no damage	30 Mar 2005	Normal	3.2	0	-0.2	Advective
frost causing no damage	7 Apr 2005	Inversion	0.8	-1	-1.6	Radiative
frost causing damage	**8 Apr 2005**	**Inversion**	**-0.6**	**-3**	**-3.2**	**Radiative**
frost causing no damage	9 Apr 2005	Normal	-1	-2.6	-2.2	Advective
frost causing no damage	10 Apr 2005	Normal	1	-1.6	-3.4	Advective
frost causing no damage	11 Apr 2005	Normal	1.6	-0.8	-1.8	Advective

Tab. 1 - Frost events during years 2003 to 2005.
Tab. 1 - Eventi di gelo negli anni dal 2003 al 2005.

air meteorological station, located inside the study area. To determine the presence or absence of temperature inversion, radiosonde reports received at midnight (00:00 local time) were used. The analysis of the vertical profile of temperature allowed the detection of thermal inversion at night. Nights with cloud cover less than 50% and wind speed less than 1.5 ms^{-1} were classified as radiative frost events. Based on these criteria, five frost events, 20th April 2003, 28th and 29th March, and 7th and 8th April 2005, were selected as radiative events, the remaining eight cases being classified as advective events.

Among the five selected frost events, damage occurred in only three of them, while no damage was reported for the others. Therefore three frost events, 20th April 2003, 28th March and 8th April 2005 were selected as the final radiative frost cases for the study.

For determining spring frost damage on apples for any frost case, the percentage of actual apple yield was divided by the expected apple yield and multiplied by one hundred. These data are surveyed by the Agricultural Insurance Company each year and for every frost event. Company officers' evaluations of frost damage are usually very accurate, being the base for refunding farmers. Protection from pests and deseases are carried out routinely in this region and most of the times there are not any other significant agents that endanger apple production in this area. Hence, if there is no frost damage, yield is little changeable from one year to another. The resolution of primary frost damage is not the same for the whole area, since farm surfaces differ one another, ranging from 1 to 5 ha. This is the information used to produce the damage map for each grid point in the area. For instance, Fig. 2 (created by observations), shows the frost damage for the 20th April 2003 event. The minimum frost damage occurred in the southeast of the study area and the maximum in southwestern parts.

2.5. Building of parameter maps

Among 12 parameters, maps of longitude, latitude, elevation above mean sea level, slope, and aspect were extracted from the Digital Elevation Model (DEM) of the Shuttle Radar Topography Mission Digital Elevation Model - DEM (NASA, 2007) with a resolution of 90 m. Maps were created for each of the other seven parameters. For the frost occurrences, the day of frost occurrence was used as a variable in the regressions. Inverse Distance Weighting (IDW) were implemented in the GIS environment for interpolation (Farajzadeh, 2008).

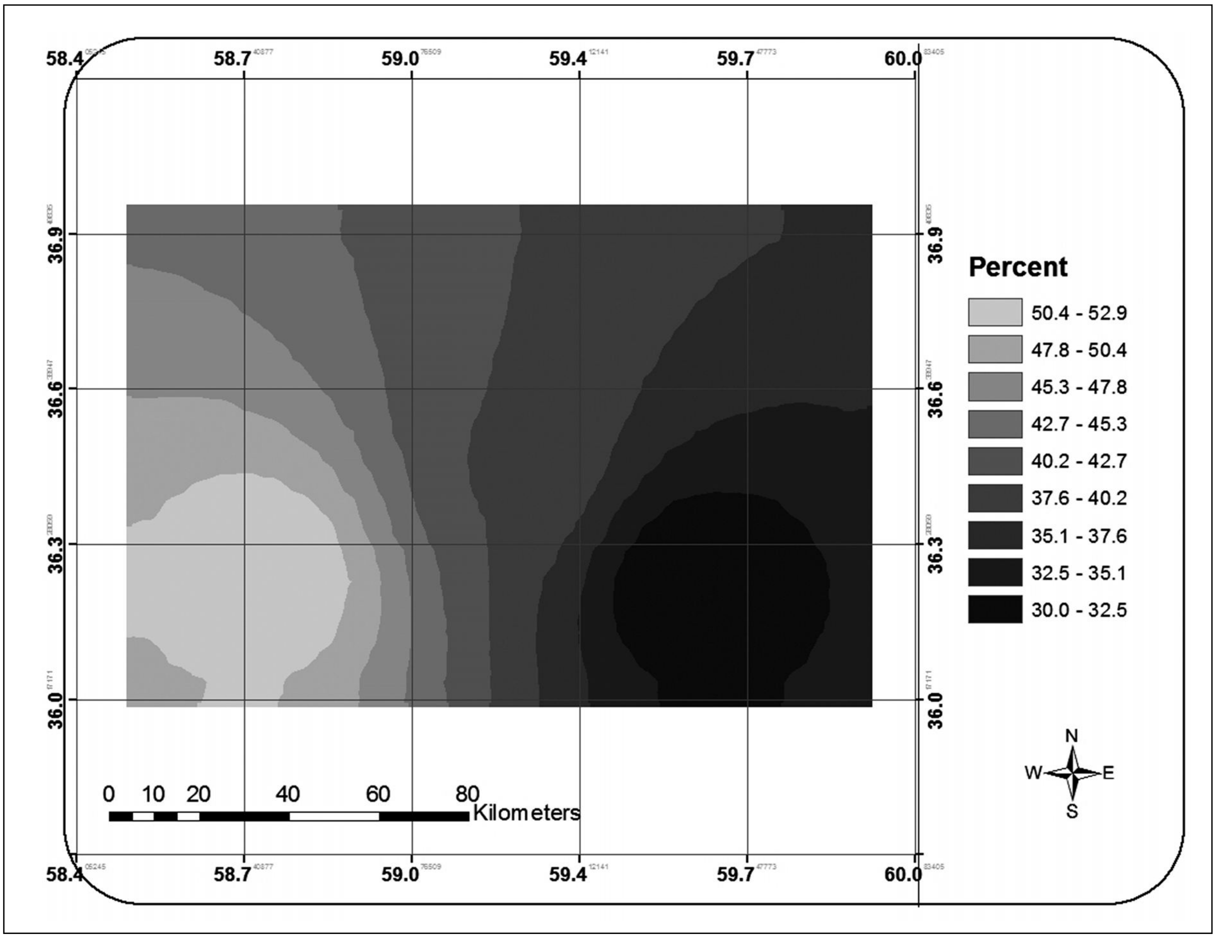

Fig. 2 - Observed frost damage for April 20th, 2003.
Fig. 2 - Danno osservato il 20 aprile 2003.

All parameters for the study area were mapped for each frost event. Spatial interpolation was done to provide enough data to input for regression. The model used these maps as inputs, and the percentage of damaged crop as output. A network of grid points with spatial resolution of 3 minutes (distance 5 km x 5 km) was overlaid on each map. The longitude and latitude axes were divided into 28 and 18 intervals, respectively, since the extent for the study region was 1.5° (longitude) by 1° (latitude). The total number of grid points was 551 (29 by 19). The values of each input and output parameter at every grid point were extracted. Finally, considering the three events, the total number of data points for regression analysis was 551 × 3 = 1653 points.

Parameter	Coefficient	Pearson Correlation
Constant	695.2	---
Longitude	-6.9	-0.23
Altitude	0.009	0.008
Minimum Temperature	-2.63	-0.383
Temperature increase rate	9.3	0.161
Temperature decrease rate	-6.9	-0.066
Area below zero line	0.39	-0.791
Cumulative Degree Days	-0.063	-0.448
Frost Date	-1.75	-1.216

Tab. 2 - Stepwise method regression coefficients and correlations.
Tab. 2 - Coefficienti di regressione e correlazioni per il metodo di regressione "stepwise".

75% of these data were picked up at random, setting up the calibration subset. The rest of data (25%) were processed for the model validation.

2.6. Modelling frosts with linear regression

For modelling and calibration of frost risk occurrences, the influence of all the 12 agents has to be quantified. Multiple regression was used to determine the impact of each of these factors, calculating Pearson correlation coefficients. Four methods of regression (Enter, Stepwise, Forward and Backward) were used to determine the coefficients of the regression equation. Root Mean Square Error (RMSE) statistics were employed for comparison of these methods (Farajzadeh, 2008).
Thus the risk of damage was estimated by using the regression analysis for three frost events based on the equation applied to each grid point. After frost damage risk was assessed for each frost event and estimated at any grid point, frost damage maps were prepared using IDW. In order to study correlations between the two maps, regression equations and correlation coefficients of each equation were obtained for each frost event.
Finally, the flow chart of methodology is sketched in Fig. 3.

3. RESULTS AND DISCUSSION

Some drivers do not to improve significantly the regression model. In order to exclude these parameters a "Stepwise regression" method was applied. The calibration results are shown in table 2, where the correlations of single variables with damage risk are reported.
The multilinear regression equation resulting from the previous analysis is the following:

$$FDR = 695.2 - 2.63Tn + 9.3\ IN - 1.75DOY + \\ + 0.39AR - 6.9DE - 0.063\ DD - 6.9X + 0.009\ Z$$

where Tn is minimum temperature, IN is temperature increase rate, DOY is the date of frost (expressed as day of the year), AR is area below zero line, DE is temperature decrease rate, DD is cumulative degree days, X is longitude and Z is elevation. RMSE of the equation was 1.72 and R^2 was 0.95. The degree of freedom was 5. The role of single drivers is commented in succession.

Minimum temperature (Tn).
Pearson Correlation coefficient between the risk of frost damage and the minimum temperature is —0.383 (significant with $p < 0.05$): as expected, the lower the temperature, the highest the damage.

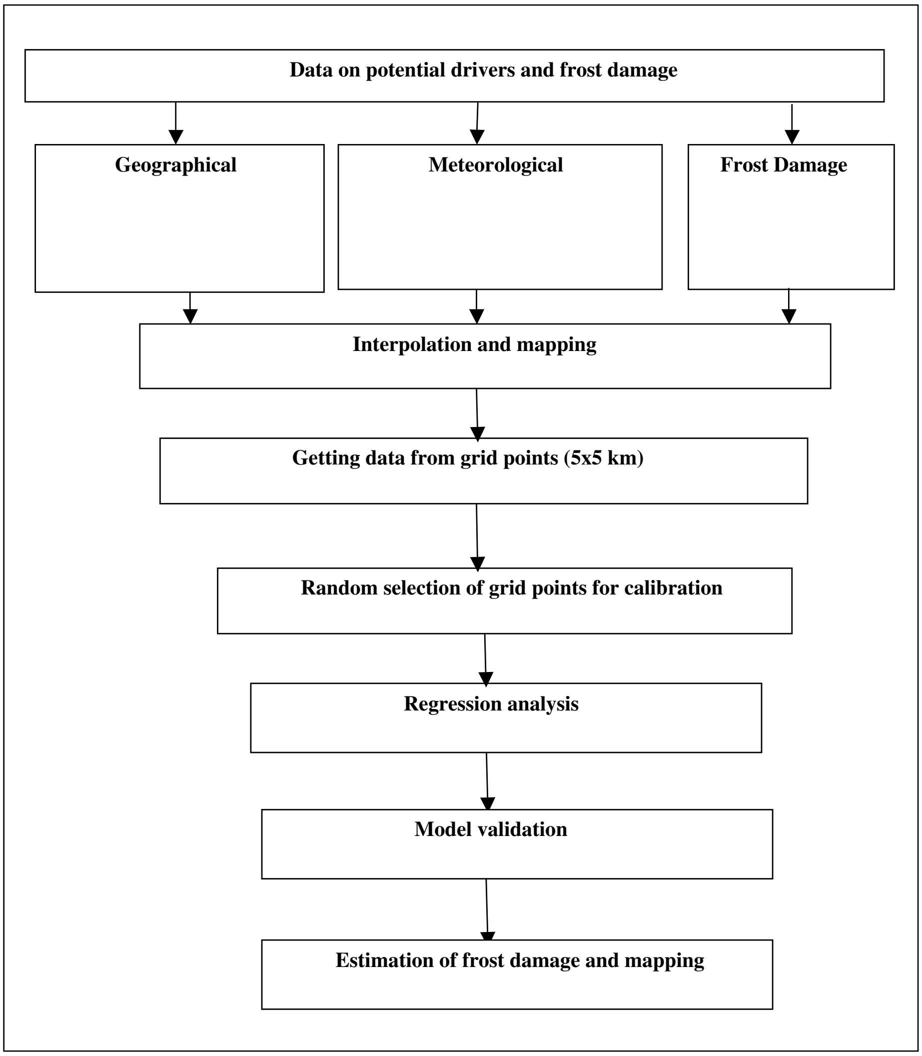

Fig. 3 - Methodology of model creation and validation.
Fig. 3 - Metodologia di creazione e validazione del modello.

Rate of temperature increase (IN)
This variable also has a positive impact on the risk of frost damage. This means that the rate of increasing temperatures after the frost event affects the amount of damage. Snyder (2005) and Ribeiro *et al.* (2006) have reached the same result. The reason for this is that slow melting of ice causes a low rate of the water loss from cells that have suffered extracellular freezing, and can therefore reduce the damage compared to a rapid melting process. If an increase in temperature after the occurrence of a frost event occurs gradually and slowly, it is better and easier for the plant to recover damaged tissues.

Day of the year (DOY)
It has a correlation coefficient equal to -1.216 with the risk of frost damage. Obviously, this negative value shows that the more advanced is the season, the lower is the risk of frost damage. The study period in this investigation was 5th to 30th April, according to the apple flowering date range. As mentioned earlier, the most critical stage of plant growth is flowering time, when the buds increase their vulnerability to frost damage. In the following stages plants do not increase sharply their susceptibility to frost, while temperature has lower and lower probability of attaining freezing values, therefore the risk of frost damage on the crop decreases.

Area below the zero line (AR)
This is the surface enclosed between the daily temperature curve and the line of daily temperature of 0 °C. This quantity has a correlation coefficient of -0.791 with frost damage, showing the direct impact of frost damage with the spread of the freezing area (the wider the below-zero area, the higher the frost damage risk). Of course, the area assumes a high

extent when both the minimum temperature is low and duration of freezing is long, each of the two components increasing the surface of below-zero terrain.

Frost duration (DU)
The correlation coefficient with the risk of damage is 0.664, which indicates the direct impact of frost duration on the amount of damage. These results confirm the findings by Snyder (2005).

Temperature decrease rate before freezing (DE)
It has a correlation coefficient equal to -0.066 with the risk of frost damage. Accordingly, the lower the rate of temperature decrease before the frost event, the greater the damage. No published work regarding the impact of temperature decrease rate before freezing has been found. What appears in this regard as a reasonable justification is the relationship between the rate of temperature decrease with the area under zero line that makes the relationship statistically significant. The lower the rate of temperature decrease to reach a certain minimum temperature, the larger will be the area under the zero line, and definitely, the bud exposure to cold.

Cumulative degree days (DD)
It has a correlation coefficient equal to -0.448 ($p < 0.05$). According to the sign of the correlation coefficient, the less heat units have been accumulated, the greater will be frost damage risk. This is an apparently counter-intuitive result, because frost tolerance decreases as the bud development proceeds. However, the probable explanation is that DD is strongly linked to the date of frost occurrence (DOY), and, in the set of frosts that were considered in this study, the ones with the lowest temperatures are also the earliest. The two independent variables, indeed, enter the regression equation with the same sign.

Longitude (X)
The correlation coefficient is equal to -0.23 for longitude ($p < 0.05$), highlighting higher risk rates at the westernmost areas of the region.

Altitude (Z)
The correlation coefficient between altitude and risk of frost damage equals 0.008 at about the 5 percent level of significance. With altitude increasing, the risk of frost damage also increases. Usually in highlands spring frosts persist later, and early autumn frosts start earlier, than in lower areas. So the frost season is longer in highlands and the frost-free period is shorter. Therefore the period with frost hazard is longer and the frost damage risk will be higher. Snyder (2005), and Loughlin and Kalma (1990) also found this relationship. However, in U- and V-shaped valleys the situation is different because the lowest part of these types of areas is often a cold-air gathering place and a cold spots forms. This leads to radiation frost conditions with cold, stable air.

Latitude (Y), slope (SL), aspect (AS)
No significant correlation was observed between the latitude, slope, and aspect of place with frost damage risk. The effects of slope and aspect on frost damages are significant at a local scale. As we worked at the mesoscale in this study, diversity and changes in slope and aspect was high and hampered significant relationships. Hijmans (1998) in a study to determine suitable areas for planting potatoes in Peru, concluded that there was no significant effect on frost damage by slope. In microscale studies of frost damage, as for a small area, the diversity of slope and aspect are not so high and these two parameters would have a statistically significant correlation.
In order to validate the model, the multilinear regression equation was applied to the 25% of data set aside for this purpose. Fig. 4 shows the correlation of observed and predicted frost damage. R^2 equals 0.84 and is significant at 5% level of probability.

4. CONCLUSIONS

This investigation studied the influences of different parameters on spring frost damage in the Mashhad plain apple cultivated area. Two categories of factors have effects on the risk, and come from meteorological and geographical characteristics of the sites. To determine the effects of potential drivers on the risk of frost damage, linear multiple regression models were built and analyzed. From 12 parameters considered, 7 are meteorological and 5 are geographical. As expected, minimum temperature was found to be the most important and most effective parameter for the frost damage risk, being directly linked with the severity of frost. Terrain slope and frost duration have little importance and seem negligible on frost damage. According to F statistics, the meteorological parameters are more important than the geographic ones. It has been postulated that apple trees have the ability to acclimate their phenological behavior (Rea and Eccel., 2006), but it is also a normal

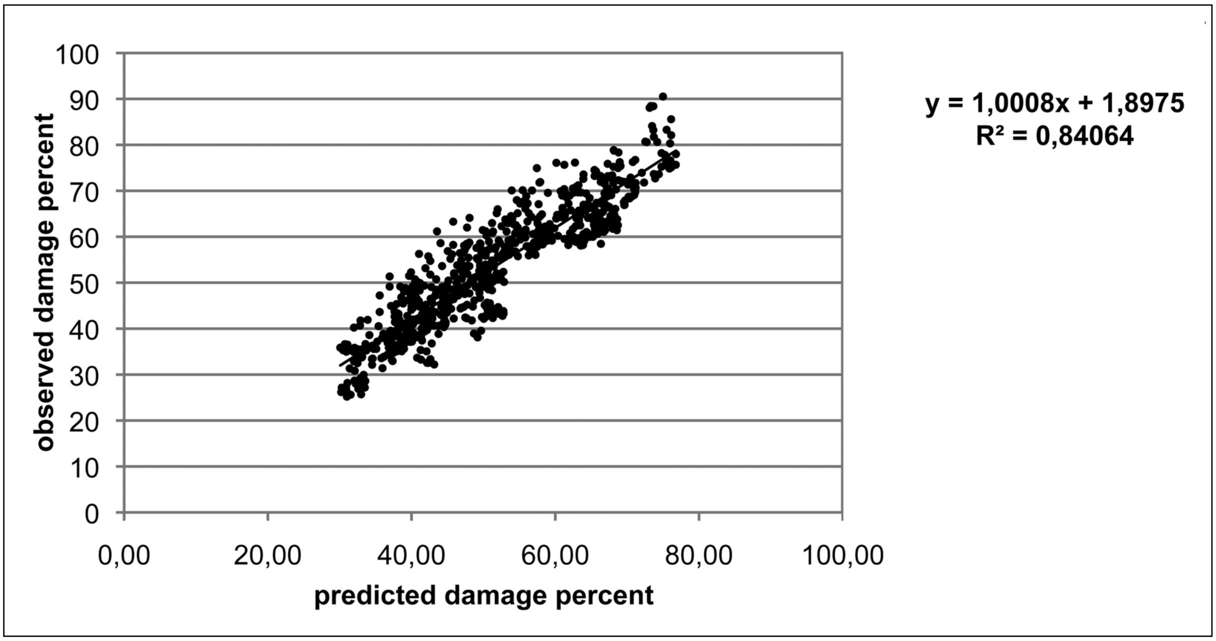

Fig. 4 - Correlation between observed and predicted frost damage (validation data set), according to the multilinear regression equation at Sect. 3 ($R^2 = 0.84$, $p < 0.05$).
Fig. 4 - Correlazione tra danno predetto ed osservato, validazione del modello, secondo l'equazione di regressione multilineare della Sez. 3 ($R^2 = 0.84$, $p < 0.05$).

feature that the lower temperatures at higher altitudes slow down the attainment of the sensitive phenological stage of flowering.

The positive verification of the regressive equation on an independent data set shows that the model is able to quantify the effects of different geographical and meteorological features on apple frost damage risk at the mesoscale in the climatic and geographic context of the region.

This kind of analysis has a general enforceability and can be applied to other natural adversities, such as, drought occurrence, or susceptibility to pest infection (Field *et al.*, 2012). Once the drivers of risk are identified, it is possible to model the response of damage to the action of drivers, aiming at the classification of areas in terms of proneness to a specific risk.

ACKNOWLEDGEMENTS

We would like to thank Nooshin Mohammadian from I.R. of Iran Meteorological Organization for preparing maps.

REFERENCES

Alizadeh A., 1995. *Applied Hydrology*. Astane Ghodss Publishing Co.: Mashhad.808 pp.

Avissar R, Mahrer Y., 1988a. Mapping frost-sensitive areas with a three-dimensional local-scale numerical model, Part I. Physical and numerical aspects. *J. Applied meteorol*. 27:400-413.

Avissar R, Mahrer Y., 1988b. Mapping frost-sensitive areas with a three-dimensional local-scale numerical model, Part II. Comparison with observations *J. Applied meteorol*. 27:414-426.

Bootsma A, 1976. Estimating minimum temperature and climatological freezing risk in hilly terrain. *Agricultural Meteorology* 16: 425-443.

Eccel E., Arman G., Zottele F., Gioli B., 2008: Il telerilevamento all'infrarosso termico per la mappatura delle temperature minime ad elevato dettaglio territoriale. (Thermal infrared remote sensing for high-resolution minimum temperature mapping). Italian Journal of Agrometeorology, 13(3):52-61

Farajzadeh M., Rahimi M., Kamali GA., Mavrommatis T., 2010. Modelling Apple Tree Bud burst time and frost risk in Iran. *Meteorological Application* 17:45-52.

Farajzadeh M., 2008. *Climatological Techniques*. SAMT publication, Tehran. 287 pp.

Field C.B., Barros V., Stocker, T.F, Qin D., Dokken D.J., Ebi K.L., Mastrandrea M.D., Mach K.J., Plattner, G.K., Allen S.K., Tignor M., Midgley P.M. (eds.), 2012: Managing the Risks of Extreme Events and Disasters to Advance Climate Change Adaptation. A Special Report of Working Groups I and II of the Intergovernmental Panel on Climate Change. Cambridge University Press, Cambridge, UK, and New York, NY, USA, 582 pp.

Hashemi F., 1977. *Climatological Requirements of Iran Main Strategic Plants*. Iran Meteorological Organization: Tehran. 129 pp.

Hijmans R.J., 1998. Estimating Frost Risk in potato Production on the Altiplano Using interpolated Climate Data. *CLP Program Report*: Peru. 380 pp.

Kajfez B.L., 1989. Early autumn frost in upper Carniola Slovenia (Yugoslavia), *Zbornik Biotechniske Univerze*: 53:19-26.

Laughlin J.P., Kalma J.D., 1990. Frost Risk mapping for landscape Planning: A methodology. *Theoretical and Applied Climatology* 42:41-51.

Lindén L., Rita H., Suojala T. 1996. Logit models for estimating lethal temperatures in apple. *HortScience* 31: 91-93.

Madelin M., Beltrando G., 2005. Spatial interpolation-based mapping of the spring frost hazard in the Champagne vineyards. *Meteorological Application* 12: 51-56.

NASA, 2007. Shuttle Radar Topography Mission (SRTM): http://www2.jpl.nasa.gov/srtm/

Porteous AS., 1996. Agrometeorology of the Apple Crop. WMO/TD-NO. 750: 3-5.

Rahimi M., Hajjam S., Khalili A., Kamali G.A., Stigter C.J. 2007. Risk analysis of first and last occurrences in the Central Alborz region. *International Journal of Climatology* 26: 349-356.

Rea R., Eccel E., 2006: Phenological models for blooming of apple in a mountainous region. International Journal of Biometeorology, Volume 51(1):1-16.

Ribeiro A.C., De Melo-Abreu J.P., Snyder R.L., 2006. Apple orchard frost protection with wind machine operation. *Agricultural and Forest Meteorology* 141:71-81.

Richards K., Baumgarten M., 2003. Towards Topoclimatic Maps of Frost and frost Risk for Scotland New Zealand. *SIRC 2003*: New Zealand.

Snyder R.L., De Melo-Abreu J.P., 2005. *Frost Protection: Fundamentals, Practice and Economics.* Vol. I.: United Nations. Food and Agriculture Organization: Rome. 240 pp.

Zinoni F., Antolini G., Campisi T., Marletto V., Rossi F., 2002. Characterisation of Emilia-Romagna region in relation with late frost risk. *Physics and Chemistry of the Earth* 27: 1091-1101.

The ARMOSA simulation crop model: overall features, calibration and validation results

Alessia Perego[1], Andrea Giussani[1], Mattia Sanna[1], Mattia Fumagalli[1], Marco Carozzi[1], Lodovico Alfieri[1], Stefano Brenna[2], Marco Acutis[1]*

Abstract: *ARMOSA is a dynamic simulation model which was developed to simulate crop growth and development, water and nitrogen dynamics under different pedoclimatic conditions and cropping systems in the arable land. The model is meant to be a tool for the evaluation of the impact of different crop management practices on soil nitrogen and carbon cycles and groundwater nitrate pollution. A large data set collected over three to six years from six monitoring sites in Lombardia plain was used to calibrate and validate the model parameters. Measured meteorological data, soil chemical and physical characterizations, crop-related data of different cropping systems allowed for a proper parameterization. Fit indexes showed the reliability of the model in adequately predicting crop-related variables, such as above ground biomass (RRMSE=11.18, EF=0.94, r=0.97), Leaf Area Index maximum value (RRMSE=8.24, EF=0.37, r=0.72), harvest index (RRMSE=19.4, EF=0.32, r=0.74), and crop N uptake (RRMSE=20.25, EF=0.69, r=0.85). Using two different one-year data set from each monitoring site, the model was calibrated and validated, getting to encouraging results: RRMSE=6.28, EF=0.52, r=0.68 for soil water content at different depths, and RRMSE=34.89, EF=0.59, r=0.75 for soil NO_3-N content along soil profile. The simulated N leaching was in full agreement with measured data (RRMSE=26.62, EF=0.88, r=0.98).*
Keywords: *simulation model, crop growth, water dynamics, nitrogen leaching, performance assessment.*

Riassunto: *ARMOSA è un modello dinamico di simulazione che è stato sviluppato per simulare la crescita colturale e le dinamiche idriche e dell'azoto in diverse condizioni pedoclimatiche. Il modello è uno strumento per la valutazione dell'impatto della gestione agronomica sul contenuto di nitrati delle acque sotterranee. Per calibrare e validare il modello è stato utilizzato un ampio set di dati misurati in sei siti di monitoraggio della pianura Lombarda. Gli indici di performance hanno mostrato l'affidabilità del modello nel predire adeguatamente le variabili riferite alla coltura (biomassa totale: RRMSE = 11.18, EF = 0.94, r = 0.97; LAI: RRMSE = 8.24, EF = 0.37, r = 0.72; harvest index: RRMSE = 19.4, EF = 0.32, r = 0.74; azoto assorbito: RRMSE = 20.25, EF = 0.69, r = 0.85). Utilizzando due diversi set di dati annuali per ciascun sito di monitoraggio, il modello è stato calibrato e validato con buoni risultati: (i) RRMSE = 6.28, EF = 0.52, r = 0.68 per il contenuto idrico del suolo a diverse profondità; (ii) RRMSE = 34.89, EF = 0.59, r = 0.75 per il contenuto di azoto nel terreno. I dati simulati medi annuali dell'azoto lisciviato sono risultati coerenti con i dati misurati (RRMSE = 26.62, EF = 0.88, r = 0,98).*
Parole chiave: *modelli di simulazione, crescita colturale, dinamica dell'acqua, lisciviazione dell'azoto, valutazione della performance.*

1. INTRODUCTION

The prediction of nitrogen content in groundwater requires knowledge of the dynamics properties of the nitrogen (N) cycle in the soil-plant-atmosphere system (Bergstrom *et al.*, 1991; Acutis *et al.*, 2000). In order to get a proper evaluation of the N balance in arable land the analysis of the soil water dynamics has first to be carried out, as water is the vector of N to groundwater (Rozemeijer *et al.*, 2010; Van der Velde *et al.*, 2010). Moreover, evaluation of the soil water content is fundamental in crop yield prediction, which plays a crucial role into the analysis of the actual sustainability of the agroecosystem (Stöckle *et al.* 1992; Kersebaum, 2007).

The complexity and interaction of physical, chemical and biological processes occurring at different space and time scale involve difficulties in evaluating water movements into the soil, attested by the physically based differential equations employed to describe the soil water dynamics. In order to solve such algorithms dynamic simulation model can be applied (Jarvis, 1989; Stöckle *et al.* 2003; Wegehenkel and Mirschel, 2006). Together with the soil water dynamic properties, detailed understanding of N dynamics is required to define a sustainable management in terms of groundwater quality.

Data from field monitoring are as well fundamental

[*] Corresponding author email: alessia.perego@unimi.it
[1] Dipartimento di Scienze Agrarie e Ambientali, Università degli Studi di Milano, Milano.
[2] Ente Regionale per i Servizi alla Agricoltura e Foreste, Milano.
Received 8 June, accepted 27 July 2013.

to test and parameterize a simulation model: once developed and tested, the simulation model can be able to predict N leaching under field crop production with high reliability (Kersebaum, 1995; Acutis *et al.*, 2000).

Different data have to be observed at field monitoring, such as (I) crop-related variables, (II) mineral N content in soil solution, (III) soil water content, (IV) agronomic management information, (V) soil characterization and (VI) meteorological data. Data set of crop variables must include phenological stages, total dry matter (above ground biomass, AGB), yield, harvest index, Leaf Area Index (LAI) maximum value. The mineral N content can be measured from soil cores or from soil solution sampled by ceramic porous cups (Lord and Sheperd, 1993; Perego *et al.*, 2012). Continuous data of soil water content can be measured by using time domain reflectometry technique (Bonfante *et al.*, 2010). Agronomic management data include sowing and harvest day, fertilization and irrigation features such as amounts, type and number of events.

The ARMOSA project (Monitoring network of soil water quality of arable land in Lombardia) was developed to define a methodology for the assessment of soil quality and nitrate vulnerability in arable systems according to the guidelines of PTUA (Program of water protection and use) of Lombardia Region (northern Italy). The main result of such project was the development of the ARMOSA dynamic model whose reliability is tested by a large set of data observed in six monitoring sites. They were in farms chosen to be representative of the ordinary and diversified pedoclimatic conditions and cropping systems characteristic of the Lombardia plain. The mean annual rainfall in this region varied from 690 to 1070 mm year^{-1}, and sites' soils were from fine sandy to clay loam. The cropping systems included silage and grain maize (*Zea mays* L.), winter wheat (*Triticum aestivum* L.), double annual crop rotation of Italian ryegrass (*Lolium multiflorum* Lam.). The mean N fertilization amounts were 304 to 642, kg N ha^{-1}year^{-1}, whereas annual irrigation was 240 to 350 mm year^{-1} (Perego *et al.*, 2012). Lombardia Region is characterized by intensive cropping systems with elevated use of production factors such as N-fertilizers and irrigation water. As a consequence, agricultural production is frequently characterized by high N surpluses as quantified in previous studies (Bechini and Castoldi, 2009; Fumagalli *et al.*, 2011). The need of developing a new model was due to the lack of available software able to simulate the entire system of soil-plant-atmosphere with high reliability. Therefore the approaches related to crop, water and N were implemented according to the state of art.

The aim of this work was to present the overall features of the ARMOSA simulation model together with the performance evaluation of the model in the calibration and the validation analysis.

2. MATERIALS AND METHODS

2.1 The ARMOSA model overview

ARMOSA is a dynamic model that simulates the cropping systems at a daily time-step at field scale, considering vertical movements of soil water and for the bottom boundary condition an unit hydraulic gradient is assumed. The software was written using the Unified Modelling Language (UML, Rumbaugh *et al.*, 2005) to have an explicit definition of its structure. The model simulates agro-meteorological variables, the water balance, the N balance, and the crop development and growth. It consists in four modules which are: I) a micro-meteorological model that simulates the energy balance, allowing the evapotranspiration estimation, II) a crop development and growth model that uses global radiation and temperature, III) a model of soil water balance, and IV) a model of soil N and carbon balance. Particularly, the water module calculates the daily soil water content and the water flux over the profile, which affect the nitrogen and carbon dynamics. The calculated variables of the evapotranspiration, soil water, nitrogen and carbon are input for the crop module, which influences in turn the daily variables of the other modules . The relation of the four modules is displayed in Fig. 1, as well as input and output data.

The ARMOSA crop simulation model was developed after a literature review of available algorithmic frames to be implemented in the software code. Particularly, the crop module is based on gross assimilation of carbon dioxide (CO_2), and on maintenance and growth respiration to get the final net carbon assimilation as implemented in SUCROS (Van Keulen *et al.*, 1982) and WOFOST models (Van Keulen and Wolf, 1986). The water dynamics can be simulated according to the physically based approach of the Richards' equation, as implemented in the SWAP model (Van Dam *et al.*, 1997; Van Dam and Feddes, 2000), or through the empirical cascading approach (Burns *et al.*, 1974). The hydraulic parameters of the Richards' approach are internally estimated from the van Genuchten parameters provided in the soil data base.

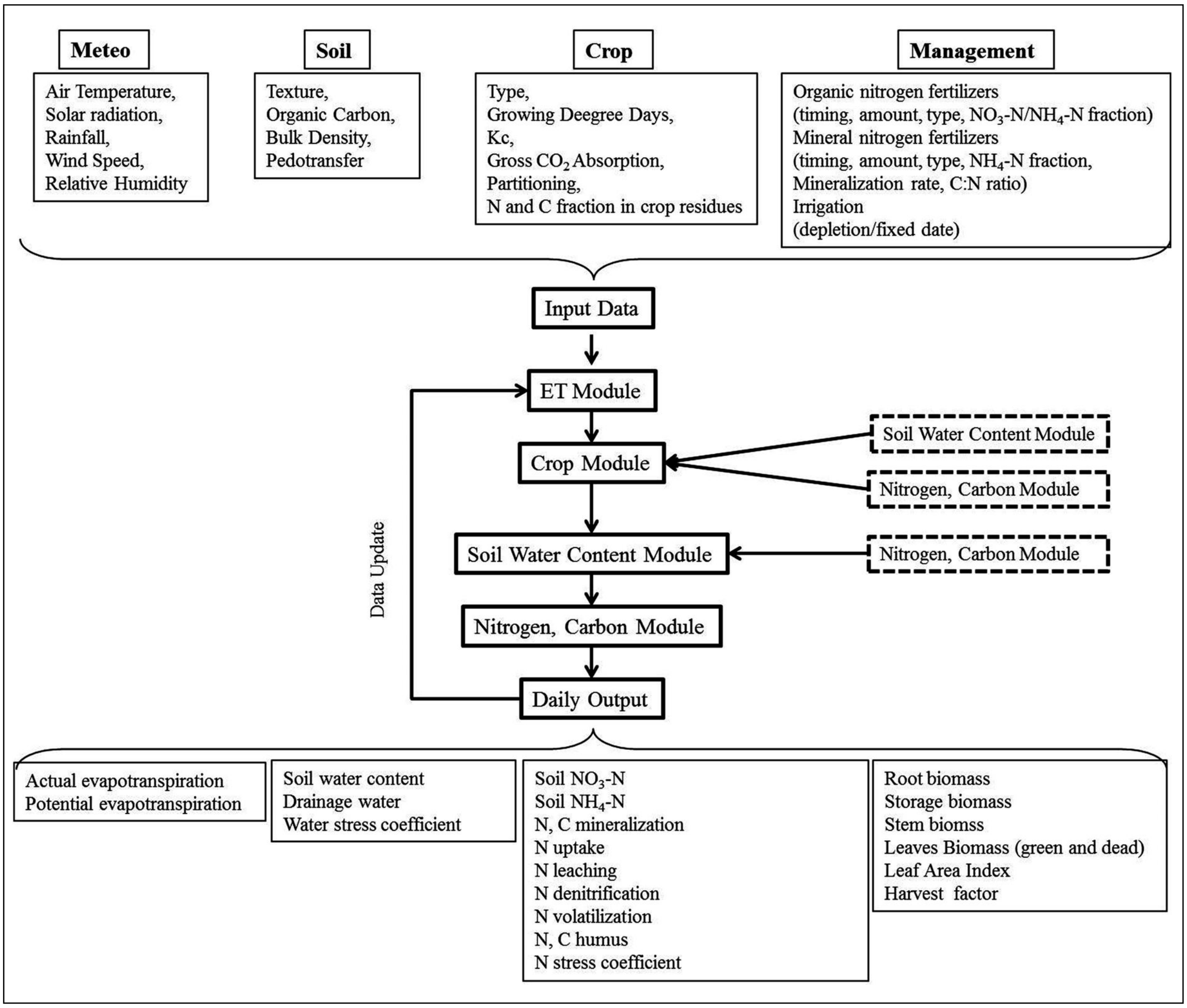

Fig. 1 - Structure overview of the ARMOSA simulation model: relationships between modules at timestep level.
Fig. 1 - Schema sintetico della struttura del modello ARMOSA: relazioni tra i diversi moduli a livello del singolo passo di simulazione.

The N dynamics module was developed on the basis of the SOILN model (Eckersten *et al.*, 1996; Larsson and Jarvis,1999) which was already implemented in other simulation models as WAVE (Vanclooster *et al.*, 1994) and LEACHN (Hutson, 2003). In particular, the latter was applied in Po plain scenario (Acutis *et al.* 2000), showing a good performance in simulating the ordinary intensive cropping systems of the studied area. Pedological parameters, as input data, are included in data base where physical parameters as texture and bulk density, chemical, as organic carbon (kg kg^{-1} soil) and carbon in the stable fraction of organic matter (kg), are reported layer by layer.
The user can define (I) crop rotation, (II) sowing and harvest time, (III) time, amount and type of N fertilizers (IV) time and amount of the irrigation events. Further, the user can choose the option of the automatic irrigation, defined by water availability threshold below whose value irrigation water is provided to ensure the field capacity content at a defined depth.
ARMOSA model also allows for selection of daily outputs for all growth and soil related variables and indicators derived from the simulation results e.g. the development stage and AGB of crops, soil water balance, as well as stress and efficiency indicators, organic carbon and N, mineral nitrogen, and water flux between layers.

2.1.1 ARMOSA: the crop module

The crop module of ARMOSA model implements STAMINA crop model (Ferrara *et al.*, 2010; Richter *et al.*, 2010), which is based on SUCROS model

(Van Keulen *et al.*, 1982). Differences between the STAMINA and the SUCROS model are in crop development, light interception, absorption model, LAI growth and water stress factor. Similar to SUCROS, ARMOSA estimates the photosynthesis for five layers along the vertical profile of the canopy, selected on the basis of a Gaussian integration, to obtain an integrated value of photosynthesis of the whole canopy. The maximum potential photosynthetic rate is a function of CO_2 concentration in the atmosphere.

Crop production is estimated under water and N limited conditions by linking growth to the soil water and N balance. The effect of water stress on plant growth is calculated as function of soil water content by using logistic function (Richter *et al.*, 2001) that simplifies the original step function proposed by Sinclair *et al.* (1987). The water stress factor (kws) is calculated at a daily time step and influences the crop-related processes such as carbohydrate production, photosynthetate partitioning and evapotranspiration (ET module). The effect of water stress on carbohydrate production is simulated considering a reduction of the absorption of CO_2 directly proportional to kws, considering the stomata closure. The water effect on partitioning reduces the amount of the net carbohydrate assimilation that in condition of no stress is used for the shoot growth, redirecting it to the roots growth only if the actual stage allows the root growth. When the root stops growing there isn't water effect on partitioning. The crop module estimates the N demand on the basis of the dilution curve as proposed by Justes et al (1994). The crop N uptake is a function of the N crop demand and of the soil availability in the root zone. The N stress factor is calculated as a function of the difference between the N crop demand and soil availability. All crop parameters, for all simulated crops and varieties, are provided in an external data base constructed in MS Access format.

2.1.2 ARMOSA: the N module

The N module was developed according to the approaches of the SOILN modul (Eckersten *et al.*, 1996; Larsson and Jarvis, 1999) with differences on attributes of the N pools. A brief description of the main N-related processes is given in this paragraph and the logical structure of the N module is shown in Fig. 2. Two mineral N pools are considered into the soil (i.e. ammoniacal and nitrate nitrogen, NH_4-N and NO_3-N). The model simulates different organic N pools being characterized by specific properties, such as C:N ratio, decomposition rate and humification rate; such diversification allows for the simulation of specific dynamic. The ARMOSA model implements three types of pool two of which are characterized by a quicker rate of decomposition (30 up to 400 days), named "litter" and "manure-derived-faeces" which represent the crop residues and the fertilizer contribution respectively. As a consequence, the organic carbon of any fertilizer application and crop residues incorporation (as function of crop type and organ) is assigned to an independent pool of the manure or litter type. The third type of N pool, humus, is the one characterized by the slower decomposition rate being the stable fraction of the organic matter in soil.

The environmental factors, such as soil temperature and water content, are involved in every N-related processes as correction factors and are calculated on the basis of reference value of the optimal condition for the microbial activity in the soil. The factors are calculated at daily time step in each soil layer. The temperature factor is expressed as a Q1O function, which generally assumes an exponential relationship with soil temperature in which Q10 is the ratio of the rate at one temperature to a temperature 10°C lower; it has been commonly used to estimate soil respiration rates from temperature (Curiel Yuste *et al.*, 2004). The soil temperature is simulated according to the approach implemented in the SWAT model (Arnold *et al.*, 1988). Two different water factors are simulated: one for the mineralization and nitrification processes and a specific one for denitrification. Both water factors are function of the soil water content at saturation. Both the mineralization and humification processes are calculated as function of specific rates, C:N ratio and the N amount in the mineral pools. The crop uptake occurs along the soil profile investigated by roots. Crop preferentially uptakes NH_4-N, if it is not available then crop uptakes NO_3-N (Watson, 1986). If available both NH_4-N and NO_3-N do not satisfy crop demand then N stress occurs. The NO_3-N Leaching is simulated according to a convection and dispersion as function of the soil water content and the N amount of the mineral pools. The nitrification process is calculated as function of the specific rate and the equilibrium NO_3-N / NH_4-N ratio. Denitrification is simulated on the basis of soil NO_3-N and water content. Ammonia volatilization occurs in the first layer as a function of soil NH_4-N and water content and its rate is maximum within the first 3 days after fertilization. Biological fixation is simulated under the leguminous cultivation and is calculated on the basis of crop N demand and NH_4-

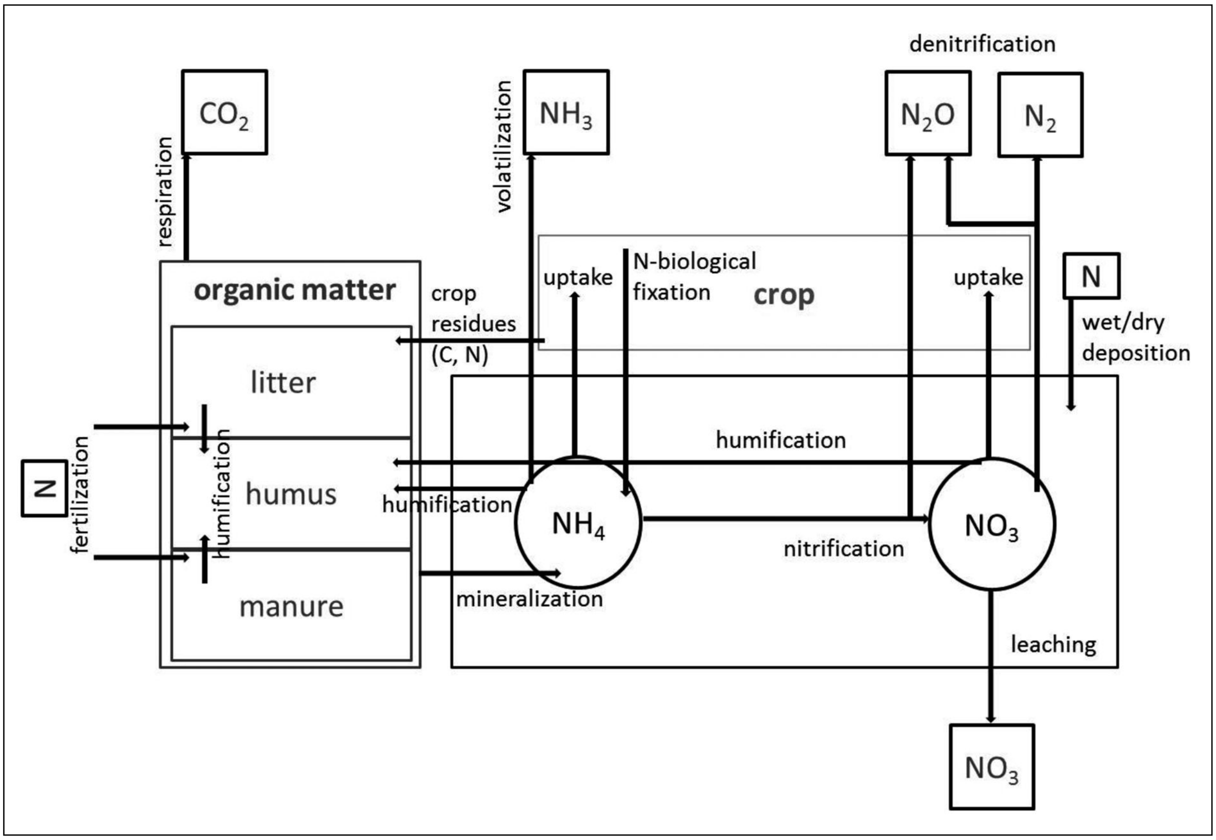

Fig. 2 - Logical structure of the nitrogen component of the ARMOSA model.
Fig. 2 - Diagramma funzionale del componente azoto del modello di simulazione ARMOSA.

N and NO_3-N availability. Dry and wet atmosphere depositions of NH_4-N and NO_3-N occur in the first layer: dry deposition is constant while wet deposition is proportional to rain fall.

2.2 Model calibration and validation

The model was calibrated and validated using the set of data collected at six monitoring sites in Lombardia plain in maize-based cropping systems (Perego *et al.*, 2012). Data sets were collected over a maximum of 5 years at 6 sites, which were sown with maize: Caviaga (LO, province of Lodi, 45.31°N, 9.50°E, 72 m a.s.l.), Cerese (MN1 and MN2, province of Mantova, 45.12°N, 10.79°E, 20 m a.s.l.), Landriano (PV, province of Pavia, 45.28°N, 9.27°E, 84 m a.s.l.), Ghisalba (BG, province of Bergamo, 45.69°N, 9.75°E, 178 m a.s.l.), Luignano (CR, province of Cremona, 45.17°N, 9.9°E, 57 m a.s.l.), all located in Lombardy plain (Fig. 3).
The soils of these six fields (LO, MN1, MN2, BG, PV, CR) were respectively *fine loamy over sandy*, *clay loam,* clay, *fine loamy, coarse silty, fine silty,* according to the USDA soil texture classification; annual rainfall ranged from 704 to 1070 mm. Organic N fertilization had an annual mean amount of 235, 498, 245, 222, 211, 0 kg N ha^{-1}year^{-1}, and mineral N mean annual amount was 118, 192, 161, 259, 103, 309 kg N ha^{-1}year^{-1} at LO, MN1, MN2, BG, PV, CR, respectively. The mean water amount which farmers applied per cropping season (from June to August) was 350 mm at BG, 300 mm at LO and CR, 280 mm at MN1 and MN2, 240 mm at PV.
Observed data of LAI, AGB and its partitioning into stem, leaf and root were collected four times during the growing cycle and at harvest; information of phenological stages were also available. The fitting indexes of above ground biomass, LAI maximum value, harvest index and total crop N uptake were calculated employing the whole data set.
The soil water content was daily measured through the soil profile (at 0.5 to 1.3 m depth) at each monitoring site by time domain reflectometry probes in two replicates; the soil solution NO_3-N concentration was measured every two weeks in two replicates by suction cups were placed at 5 depths (at 0.3 to 1.3 m depth). The performance of model was assessed on a set

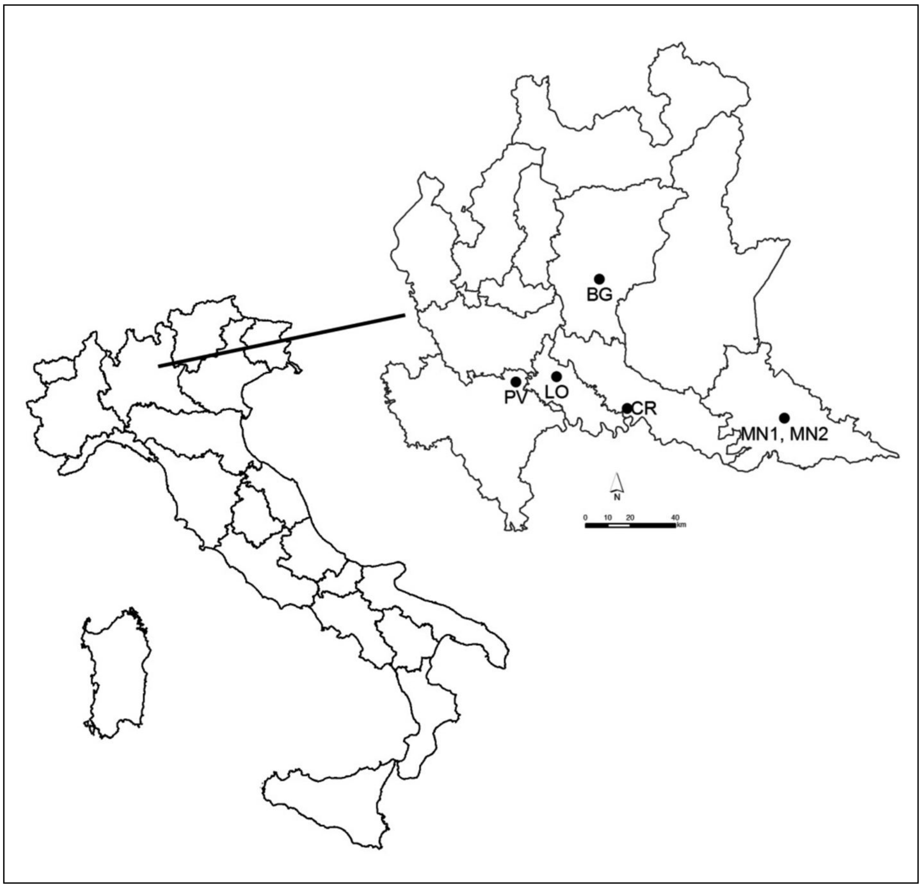

Fig. 3 - Location of the six monitoring sites in Lombardia plain (Northern Italy).
Fig. 3 - Localizzazione dei sei siti di monitoraggio nella pianura lombarda (nord Italia).

of 6100 data of water content measured at 0.5 to 1.3 m depth and 950 data of NO_3-N concentration in soil solution collected at 0.3 to 1.3 m depth. The model was calibrated and validated on one-year sets of data of each monitoring site. Tab. 1 reports calibration and validation years and monitoring depths of soil water content and NO_3-N concentrations. Six crops were parameterized, such as grain maize of 700 FAO class, grain maize of 600 FAO class, silage maize of 700 FAO class, silage maize of 500 FAO class, winter wheat, and Italian ryegrass. Reference values for crop calibration are taken from the parameter set proposed by Van Heemst (1988) for the SUCROS model simulation of grain and silage maize, winter wheat and Italian ryegrass, with the exception of phenological development parameters. In fact phenological parameters proposed by van Heemst were appropriate for crops in northern Europe but not suitable for mild temperature of the studied area, where GDD (Growing Degree Days) sum is higher, as well as the cardinal

	calibration year	validation year	depth [m]				
LO	2002	2003	0.3	0.5	0.8	1.2	1.4
MN1	2002	2003	0.3	0.5	0.7	1.0	1.3
MN2	2005	2006	0.3	0.5	0.7	1.0	1.3
BG	2005	2006	0.4	0.7	0.9	1.2	1.3
PV	2006	2008	0.3	0.5	0.8	1.0	1.3
CR	2005	2006	0.4	0.5	0.8	1.0	1.5

Tab. 1 - Calibration and validation years for each of the six monitoring sites in Lombardia plain; acquisition depths are also reported.
Tab. 1 - Dati utilizzati in fase di calibrazione e validazione dei parametri relativi alle dinamiche idriche e azotate nei sei siti di monitoraggio in pianura lombarda; sono riportate le profondità di misurazione.

temperature for CO_2 assimilation. The parameterization of the GDD requirement was performed on the basis of the field observation of development stages. Other sources for the parameterization were reported in the STAMINA project report (Richter *et al.* 2006) subsequently used by Ferrara *et al.* (2010) and Richter *et al.* (2010). Crop coefficient for the ET parameterization was suggested by FAO 56 book (Allen *et al.*, 1998). Parameters related to N dilution curve were set according to Plénet and Lemaire (2000) for grain maize, to Herrmann and Taube (2004) for silage maize, to Justes *et al.* (1994) for winter wheat from which the parameters of the Italian ryegrass crop were derived. Parameters of N-related processes were first set using reference data, mainly obtained from literature, searching for experimental data carried out in northern Italy under similar agronomic condition (Grignani *et al.*, 2003). Hydraulic parameters of the van Genuchten curve were obtained by measurements carried out in laboratory on undisturbed soil cores for each monitoring sites (Acutis *et al.*, 2007). A fitting of calculated data of NO_3-N leaching amount at monitoring sites and simulated data was carried out. Leaching losses were calculated as described by Perego *et al.* (2012) who used the method proposed by Lord and Shepherd (1993).

2.3 Evaluation of the model performance

The agreement between observed and simulated values was expressed by the indexes proposed by Loague and Green (1991) and more recently discussed by Fila *et al.* (2003) and Rocca *et al.* (2013): the relative root mean squared error (RRMSE), the coefficient of residual mass (CRM), the Pearson correlation (r), slope index and modelling efficiency (EF). RRMSE (Loague and Green, 1991) has a minimum and optimum value at 0. It is a difference-based measure of the model performance in a quadratic form divided by observed mean, being a relative measure of the fitting [1].

$$RRMSE = \frac{\sqrt{\dfrac{\sum_{i=1}^{n} (S_i - O_i)^2}{n}}}{\overline{O}} \times 100 \qquad [1]$$

Positive values of CRM indicate an underestimation of the model outcome, while values close to zero indicate the absence of trends [2].

$$CRM = \frac{\sum_{i=1}^{n} O_i - \sum_{i=1}^{n} S_i}{\sum_{i=1}^{n} O_i} \qquad [2]$$

The coefficient of correlation r (Addiscott and Whitmore, 1987) has its optimum value to maximum (+1) values; zero means no correlation [3].

$$r = \frac{\sum_{i=1}^{n} (O_i - \overline{O})(S_i - \overline{S})}{\sqrt{\sum_{i=1}^{n} (O_i - \overline{O})^2} \sqrt{\sum_{i=1}^{n} (S_i - \overline{S})^2}} \qquad [3]$$

The slope is an index quantifying the steepness of the linear regression [4].

$$slope = \frac{\sum_{i=1}^{n} (O_i - \overline{O})(S_i - \overline{S})}{\sum_{i=1}^{n} (O_i - \overline{O})^2} \qquad [4]$$

The EF index (Nash and Sutcliffe, 1970) assumes a maximum and optimum value equal to 1 and it can get either positive or negative values. EF values lower than 0 result from a worse fit than the average of measurements [5].

$$slope = \frac{\sum_{i=1}^{n} (O_i - \overline{O})(S_i - \overline{S})}{\sum_{i=1}^{n} (O_i - \overline{O})^2} \qquad [5]$$

For all the indexes O_i is the i^{th} observed value, S_i is the estimated i^{th} value and n is the number of data pairs. and are the mean of observed and simulated quantities, respectively.

3. RESULTS

3.1 Simulation of crop-related variables

The ARMOSA model showed a good performance in simulating crop-related variables. Tab. 2 reports observed and simulated data of AGB (kg ha^{-1}) and crop N uptake (kg N ha^{-1}) scored at each monitoring site. Tab. 3 shows the evaluation indexes for different crop-related variables such as (I) AGB, (II) LAI maximum value, scored at flowering stage, (III) harvest index, HI, obtained as crop yield and AGB ratio, and (IV) crop N uptake.

			Dry matter [kg ha^{-1}]			N Uptake [kg N ha^{-1}]			
Site	date	crop	observed	SE	simulated	Observed	SE	simulated	time
LO	19/8/02	MF 700	22964	1301	21740	220	33	187	harvest
	5/8/03	MF 700	15508	734	20110	147	32	210	harvest
	19/8/04	MF 700	18747	208	18670	212	18	194	harvest
	7/7/05	MF 700	11157	593	10143	133	14	126	flowering
	17/8/05	MF 700	18415	1041	19110	201	19	224	harvest
	27/6/06	WW	15833	658	13820	190	6	181	harvest
MN1	20/9/02	MG 700	32495	1726	28610	425	43	333	harvest
	7/8/03	MF 700	28037	1042	26450	290	14	262	harvest
	18/8/04	MG 600	20482	1088	21690	198	10	195	harvest
MN2	23/9/05	MG 700	26550	1179	24310	289	25	228	harvest
	5/9/06	MG 700	28123	621	28250	289	18	269	harvest
BG	19/10/05	MG 600	22522	126	22480	197	11	219	harvest
	20/9/06	MF 700	22934	103	21980	236	7	238	harvest
	26/9/08	MG 600	23815	1265	24440	234	24	253	harvest
	25/9/09	MF 700	26454	1078	23890	280	13	251	harvest
PV	6/5/05	It.R	6375	339	6870	84	8	41	harvest
	2/8/05	MF 700	10391	552	10992	153	10	137	flowering
	18/10/05	MF 700	20241	1075	21210	195	22	216	harvest
	11/9/06	MG 700	22764	1209	24600	235	26	188	harvest
	10/5/08	It.R	4997	996	4520	69	6	46	harvest
	25/9/08	MF 500	20993	1115	20620	163	11	280	Harvest
	10/5/09	It.R	6703	1548	5950	94	8	51	Harvest
	23/9/09	MF 500	21930	1165	20610	222	16	277	Harvest
CR	7/7/05	MG 700	14232	756	13323	198	18	198	Flowering
	27/9/05	MG 700	27861	145	29950	293	21	302	Harvest
	22/8/06	MF 700	16779	653	16630	151	24	144	Harvest

Tab. 2 - Observed and simulated data of crop above ground dry matter and crop N uptake. Acquisition date and standard error (SE) of the observed data are also reported. Grain maize of 700 FAO class (MG 700), grain maize of 600 FAO class (MG 600), silage maize of 700 FAO class (MF 700), silage maize of 500 FAO class (MF 500), winter wheat (WW), Italian ryegrass (It.R).

Tab. 2 - Dati osservati e simulate della biomassa vegetale secca e del suo contenuto in azoto. Sono riportate le date di acquisizione del dato e l'errore standard (SE). Mais da granella, classe FAO 700 (MG 700), mais da granella, classe FAO 600 (MG 600), mais da foraggio, classe FAO 700 (MF 700), mais da foraggio, classe FAO 500 (MF 500), frumento tenero (WW), loiessa (It.R).

	RRMSE	CRM	r	slope	EF
Crop above ground dry matter	11.18	0.01	0.97	0.94	0.94
LAI maximum value	8.24	-0.04	0.72	0.42	0.37
Harvest Index	19.40	-0.05	0.74	0.59	0.32
Crop N uptake	20.25	0.03	0.85	0.83	0.69

Tab. 3 - Evaluation indexes of model performance in simulating crop-related variables. RRMSE is the relative root mean square error; CRM is the coefficient of residual mass; r is the Pearson correlation coefficient; EF is the modelling efficiency.
Tab. 3 - Indici di valutazione del modello ARMOSA nel predire variabili relative alla crescita colturale nei siti di monitoraggio. RRMSE è l'errore quadratico medio relativo; CRM è il coefficiente di massa residuale; r è il coefficiente di correlazione di Pearson; EF è l'efficienza di modellizzazione.

Different evaluation indexes had scores close to optimal value, especially for AGB and crop N uptake. Although slope values for LAI and Harvest Index were not sufficiently close to optimal value, CRM and EF indexes showed a strong reliability of ARMOSA model in predicting data. Fitting was carried out by employing data observed at flowering and maturity stage in order to confirm the good performance of the model over the whole crop development.

3.2 Simulation of soil water and NO_3-N content

The evaluation of the model performance in simulating soil water content and NO_3-N concentration was carried out by using two different data set in order to first calibrate the parameterization and then to validate it.

Results of the water content fitting between observed and simulated values of each monitoring site are reported in Tab. 4. The remarkable values showed a good performance of the model at different depths, scoring always positive values in the case of EF index. The outstanding result was that the fitting values remained confident passing from the calibration to the validation year. In fact no remarkable difference was highlighted at every monitoring depths and sites. Since the water data set collected at the CR site was not complete, this evaluation was not performed. The observed and simulated data of soil water content for the calibration and validation steps are displayed in a scatter plot in Fig. 4.

Tab. 5 reports the evaluation results of the model performance in predicting soil NO_3-N concentration at different depths and sites. Values showed a complete agreement between measured and simulated data with no evident decreasing in model performance from calibration to validation years. Such result confirmed the reliability of the model in assessing soil NO_3-N concentration. CRM resulted often close to optimal value of 0, whereas EF had positive value in every cases. On average the value of coefficient r was satisfying, although in some cases values lower than 0.6 were obtained. In particular, the r of the bottom layer at the BG site had an insufficient value, scoring 0.37 and 0.33 in the calibration and validation year, respectively. However an overall good performance of the model

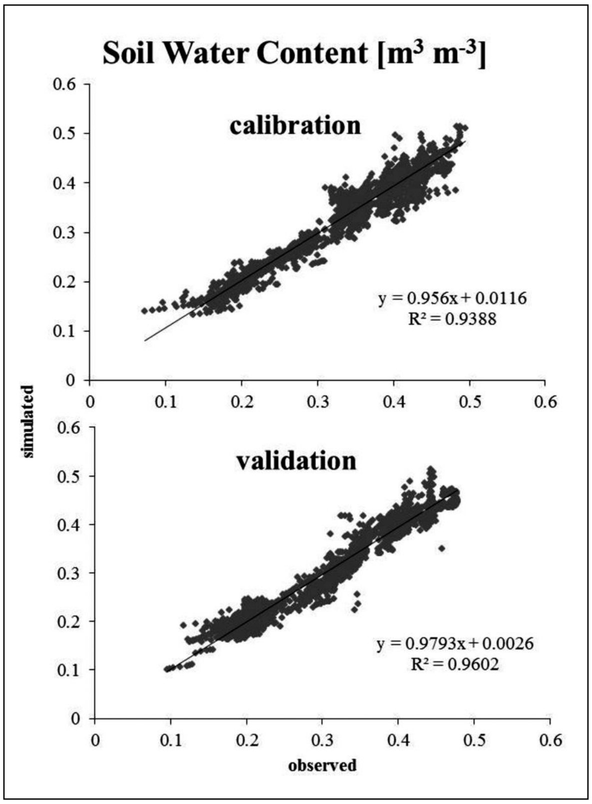

Fig. 4 - Scatter plot between observed and simulated data of soil water content of the six monitoring sites in Lombardia plain. Calibration and validation data are separately presented they concern four monitoring depths (0.5 to 1.4 m).
Fig. 4 - Accordo tra i dati simulati e misurati delle concentrazioni di azoto nitrico della soluzione circolante dei suoli nei sei siti di monitoraggio della pianura lombarda. I dati di calibrazione e validazione sono presentati separatamente e comprendono i dati relativi a quattro diverse profondità (da 0.5 fino a 1.4 m).

	LO			MN1			MN2			BG			PV		
	depht [m]	2002	2003	depht [m]	2002	2003	depht [m]	2005	2006	depht [m]	2005	2006	depht [m]	2006	2008
RRMSE	0.5	11.41	2.68	0.5	6.94	8.91	0.5	4.00	5.41	0.4	10.17	11.16	0.5	7.11	6.06
	0.8	5.55	9.25	0.7	5.90	6.94	0.7	2.40	2.36	0.7	17.65	16.95	0.8	0.89	1.50
	1.2	1.08	3.21	1.0	5.70	7.98	1.0	3.05	1.18	0.9	4.79	6.80	1.0	7.50	4.39
	1.4	5.74	11.67	1.3	10.35	9.69	1.3	1.30	1.26	1.2	19.64	17.65	1.3	0.71	5.22
CRM	0.5	0.06	0.01	0.5	0.06	0.01	0.5	0.01	0.09	0.4	0.00	0.00	0.5	0.01	0.02
	0.8	0.03	0.08	0.7	0.04	0.06	0.7	0.00	0.00	0.7	0.00	0.01	0.8	0.00	0.01
	1.0	-0.01	0.01	1.0	0.02	0.01	1.0	-0.02	0.00	0.9	0.00	-0.02	1.0	-0.07	-0.05
	1.3	-0.04	0.03	1.3	0.04	-0.04	1.3	0.00	-0.01	1.2	0.03	0.06	1.3	0.08	0.08
r	0.5	0.64	0.96	0.5	0.79	0.43	0.5	0.83	0.69	0.4	0.66	0.54	0.5	0.75	0.76
	0.8	0.45	0.74	0.7	0.91	0.79	0.7	0.67	0.59	0.7	0.75	0.62	0.8	0.46	0.71
	1.0	0.99	0.69	1.0	0.79	0.86	1.0	0.47	0.69	0.9	0.77	0.76	1.0	0.23	0.29
	1.3	0.69	0.68	1.3	0.83	0.78	1.3	0.75	0.40	1.2	0.71	0.71	1.3	0.80	0.69
slope	0.5	0.54	0.95	0.5	0.57	0.51	0.5	1.22	0.92	0.4	0.79	0.41	0.5	0.63	0.62
	0.8	0.52	1.17	0.7	1.11	0.57	0.7	1.02	0.84	0.7	0.98	1.45	0.8	0.35	0.49
	1.0	1.05	0.63	1.0	0.74	0.61	1.0	0.70	0.60	0.9	0.77	0.65	1.0	0.23	0.29
	1.3	0.69	0.68	1.3	0.53	0.77	1.3	1.00	0.37	1.2	0.49	0.49	1.3	0.46	0.41
EF	0.5	0.77	1.00	0.5	0.56	0.23	0.5	0.22	0.01	0.4	0.41	0.25	0.5	0.35	0.28
	0.8	0.42	0.99	0.7	0.55	0.56	0.7	1.00	1.00	0.7	0.24	0.38	0.8	1.00	0.98
	1.0	0.97	0.30	1.0	0.45	0.49	1.0	0.07	0.42	0.9	0.53	0.51	1.0	0.83	0.92
	1.3	0.52	0.37	1.3	0.33	0.22	1.3	0.25	0.09	1.2	0.43	0.70	1.3	0.56	0.46

Tab. 4 - Statistical indexes of model performance in simulating soil water content from 0.5 to 1.3 m depth. For each monitoring site statistical indexes are referred to the annual data sets, respectively of calibration and validation. Specific acquisition depths are also reported. RRMSE is the relative root mean square error; CRM is the coefficient of residual mass; r is the Pearson correlation coefficient; EF is the modelling efficiency.

Tab. 4 - Indici di valutazione del modello ARMOSA nel predire il contenuto idrico del suolo nei diversi strati nei siti di monitoraggio. Gli indici si riferiscono all'analisi statistica condotta sui data set annuali di calibrazione e validazione. Sono riportate le profondità di misurazione. RRMSE è l'errore quadratico medio relativo; CRM è il coefficiente di massa residuale; r è il coefficiente di correlazione di Pearson; EF è l'efficienza di modellizzazione.

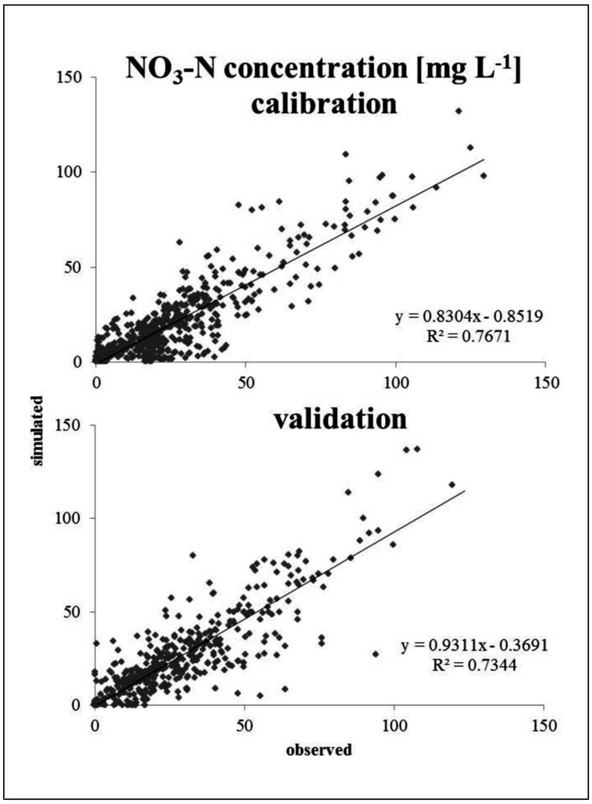

Fig. 5 - Scatter plot between observed and simulated data of NO_3-N concentration of soil solution in the six monitoring sites in Lombardia plain. Calibration and validation data are separately presented and they concern five monitoring depths (0.3 to 1.5 m).

Fig. 5 - Accordo tra i dati simulati e misurati delle concentrazioni di azoto nitrico della soluzione circolante dei suoli nei sei siti di monitoraggio della pianura lombarda. I dati di calibrazione e validazione sono presentati separatamente e comprendono i dati relativi a cinque diverse profondità (da 0.3 fino a 1.5 m).

also in the case of BG at bottom layer was confirmed by the satisfying values of Slope (0.47 and 0.71),CRM (0.07 and 0.22) and EF (0.21 and 0.19). Fig. 5 shows the agreement between the observed and simulated data of NO_3-N concentration of the calibration and validation steps.

3.3 The NO_3-N leaching simulation

The agreement between calculated and simulated data was tested employing annual leaching data from the monitoring sites. The outcome of the match was encouraging, since the evaluation indexes were close to optimal values: RRMSE=26.62, CRM=-0.06, r=0.98 , slope=1.24 and EF=0.88. CRM, whose value was negative, although close to zero, indicated a slightly overestimation of the model in simulating N leaching. Fig. 2 shows the linear regression of leaching data. The calculated slope was significantly different from 1 ($p<0.05$) which is the best obtainable value. When the 2004 N leaching data of the MN1 site was not included in the regression analysis, then slope value got a better value which did not statistically differ from the best score 1 ($p>0.05$). In fact, the 2004 value of NO_3-N in MN1 was particularly high (321 kg ha^{-1}) and, as consequence, it was out of the interpolation range.

4. DISCUSSION

The calculated fit indexes confirmed a remarkable model performance in predicting above ground biomass, crop N uptake, soil water content, soil NO_3-N concentration at different layers, and N leaching. Existing modelling calibration carried out under similar condition gave same or worse results, compared to the ARMOSA model performance.

Bechini *et al.* (2006) parameterized CropSyst model (Stöckle *et al.*, 2003) for winter wheat crop by using data set of four monitoring sites in the Lombardia plain. Among the reported fit indexes RRMSE (9 to 32), EF (0.57 to 0.98), slope (0.61 to 1.09), r (0.89 to 0.99) were in agreement with the one we calculated for AGB. Also for crop N uptake fit indexes were in agreement, being RRMSE 8 to 28, EF -0.29 to 0.95, slope 0.32 to 1.04, r 0.5 to 0.99.

Fernandez *et al.* (2002) evaluated the WAVE 2.1 (Vanclooster *et al.*, 1996) and the EURO-ACCESS-II (Armstrong *et al.*, 1996) models soil water content in a cropped soil under Mediterranean conditions; average EF was equal to -6 and -3.5 during the model calibration and validation, respectively. Bonfante *et al.* (2010) compared SWAP (Van Dam *et al.*, 1997), CropSyst (Stöckle *et al.*, 2003) and MACRO (Larsbo and Jarvis, 2003) models to predict soil water content under a maize cropping systems at two sites in Lombardia plain. EF was -0.45 to 0.42, r was 0.39 to 0.79, whereas CRM value was always close to zero. Under maize cropping systems in Po valley, Morari and Giupponi (1997) estimated N leaching by using the GLEAMS (Arnold *et al.*, 1990). The agreement between observed and simulated data was confirmed by r of 0.96 and slope 0.91.

Kersebaum and Beblik (2001) evaluated HERMES (Kersebaum, 1995) in predicting mineral N content in the root zone on single fields (A) of a water catchment in Germany and their average values separated for cropping systems (B). In A comparison r and slope resulted 0.54 and 0.64, whereas in B comparison r and slope were 0.87 and 1.24.

Eventually, the robustness index (I_R, Confalonieri *et al.*, 2010) was calculated to quantify the reliability

	LO			MN1			MN2			BG			PV			CR		
	depht [m]	2002	2003	depht [m]	2002	2003	depht [m]	2005	2006	depht [m]	2005	2006	depht [m]	2006	2008	depht [m]	2005	2006
RRMSE	0.3	21.11	70.00	0.3	17.41	43.61	0.3	84.35	69.44	0.4	46.98	15.68	0.3	17.55	67.82	0.4	23.47	5.19
	0.5	20.17	35.45	0.5	17.46	26.20	0.5	58.60	57.42	0.7	56.06	23.42	0.5	19.42	69.01	0.5	22.68	10.87
	0.8	18.09	21.41	0.7	34.34	50.59	0.7	22.05	15.69	0.9	81.00	69.00	0.8	18.45	49.51	0.8	29.02	30.57
	1.2	20.20	33.95	1.0	30.34	32.75	1.0	19.80	13.91	1.2	28.83	27.99	1.0	30.90	48.81	1.0	44.77	41.99
	1.4	16.84	38.67	1.3	30.84	34.29	1.3	28.02	1.84	1.3	64.60	40.32	1.3	40.63	19.29	1.5	31.65	32.87
CRM	0.3	0.25	0.25	0.3	0.03	0.12	0.3	-0.18	0.21	0.4	0.04	0.03	0.3	0.08	0.46	0.4	0.13	0.11
	0.5	0.06	0.15	0.5	0.19	-0.09	0.5	-0.20	0.02	0.7	0.28	0.40	0.5	0.27	0.64	0.5	0.09	0.21
	0.8	-0.03	0.07	0.7	0.10	-0.03	0.7	0.14	0.11	0.9	0.16	0.52	0.8	0.12	0.47	0.8	0.16	0.03
	1.2	0.45	0.17	1.0	0.24	0.00	1.0	0.35	-0.07	1.2	0.18	0.08	1.0	0.41	0.19	1.0	-0.01	-0.01
	1.4	0.39	0.20	1.3	0.14	0.07	1.3	0.11	0.04	1.3	0.07	0.22	1.3	0.00	0.70	1.5	0.01	0.01
r	0.3	0.74	0.70	0.3	0.62	0.55	0.3	0.74	0.76	0.4	0.73	0.57	0.3	0.69	0.73	0.4	0.65	0.50
	0.5	0.95	0.67	0.5	0.75	0.91	0.5	0.70	0.71	0.7	0.84	0.64	0.5	0.59	0.90	0.5	0.74	0.85
	0.8	0.78	0.82	0.7	0.62	0.72	0.7	0.75	0.69	0.9	0.76	0.59	0.8	0.44	0.94	0.8	0.96	0.97
	1.2	0.93	0.85	1.0	0.83	0.70	1.0	0.77	0.99	1.2	0.76	0.85	1.0	0.49	0.49	1.0	0.94	0.85
	1.4	0.88	0.82	1.3	0.72	0.90	1.3	0.77	0.82	1.3	0.37	0.33	1.3	0.55	0.94	1.5	0.68	0.87
slope	0.3	0.52	0.72	0.3	0.70	0.34	0.3	0.58	0.55	0.4	0.73	0.57	0.3	0.69	0.68	0.4	0.50	0.50
	0.5	0.68	0.49	0.5	0.64	0.70	0.5	0.54	0.55	0.7	0.84	0.64	0.5	0.59	0.90	0.5	0.85	0.85
	0.8	0.77	0.73	0.7	0.62	0.65	0.7	0.70	0.72	0.9	0.72	0.60	0.8	0.44	0.93	0.8	0.97	0.97
	1.2	1.08	1.17	1.0	0.70	0.97	1.0	0.41	0.40	1.2	0.74	0.85	1.0	0.49	0.44	1.0	0.77	0.85
	1.4	0.98	1.06	1.3	0.85	1.43	1.3	0.85	0.70	1.3	0.47	0.71	1.3	0.55	0.94	1.5	0.68	0.71
EF	0.3	0.33	0.38	0.3	0.10	0.24	0.3	0.50	0.43	0.4	0.44	0.16	0.3	0.44	0.17	0.4	0.21	0.22
	0.5	0.85	0.46	0.5	0.25	0.79	0.5	0.42	0.47	0.7	0.39	0.18	0.5	0.68	0.15	0.5	0.45	0.55
	0.8	0.57	0.73	0.7	0.13	0.47	0.7	0.38	0.29	0.9	0.24	0.16	0.8	0.77	0.69	0.8	0.94	0.93
	1.2	0.30	0.28	1.0	0.10	0.05	1.0	0.74	0.65	1.2	0.23	0.61	1.0	0.58	0.21	1.0	0.33	0.46
	1.4	0.31	0.23	1.3	0.11	0.25	1.3	0.39	0.22	1.3	0.21	0.19	1.3	0.30	0.39	1.5	0.71	0.75

Tab. 5 - Evaluation indexes of model performance in simulating soil NO_3-N concentrations from 0.3 to 1.5 m depth. For each monitoring site statistical indexes are referred to the annual data sets, respectively of calibration and validation. Specific acquisition depths are also reported. RRMSE is the relative root mean square error; CRM is the coefficient of residual mass; r is the Pearson correlation coefficient; EF is the modelling efficiency.

Tab. 5 - Indici di valutazione del modello ARMOSA nel predire la concentrazione di N-NO_3 nella soluzione circolante nei diversi strati nei siti di monitoraggio. Gli indici si riferiscono all'analisi statistica condotta sui data set annuali di calibrazione e validazione. Sono riportate le profondità di misurazione. RRMSE è l' errore quadratico medio relativo; CRM è il coefficiente di massa residuale; r è il coefficiente di correlazione di Pearson; EF è l'efficienza di modellizzazione.

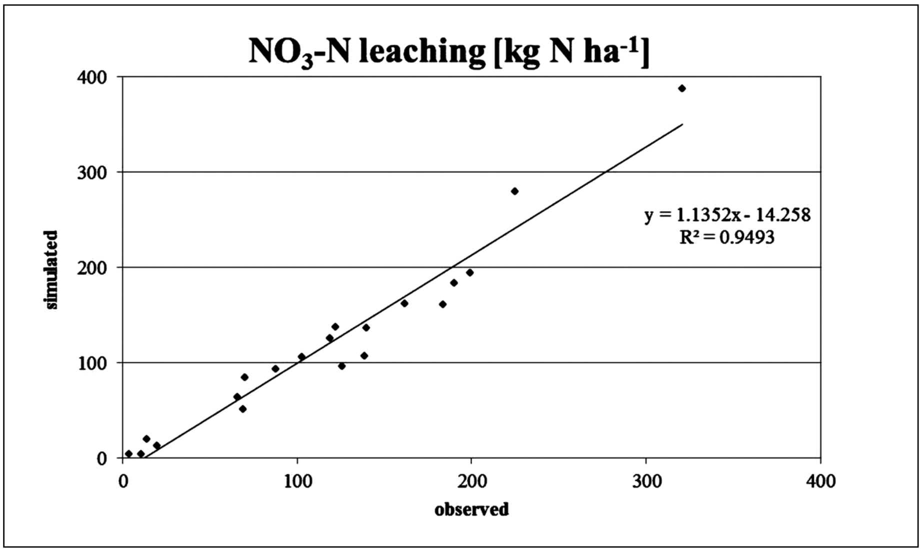

Fig. 6 - Regression line between observed and simulated data of annual N leaching (kg N ha^{-1}) of the six monitoring sites in Lombardia plain.
Fig. 6 - Regressione lineare tra i dati simulati e misurati dell'azoto medio annuale lisciviato nei sei siti di monitoraggio della pianura lombarda.

of the ARMOSA model in simulating the soil water content and the NO_3-N concentration. The I_R was first calculated as ratio between the standard deviation of the EF of soil water content data and the standard deviation of the values of the normalized Synthetic AgroMeteorological indicator (SAM), which is based on cumulated rainfall and reference evapotranspiration to characterize the climate conditions.
The calculated I_R was 1.99 while the I_R based on the EF of NO_3-N concentrations was 1.51. The latter value was compared to the I_R calculated as ratio between the standard deviation of the EF of NO_3-N concentrations and the standard deviation of the values of SAM based on N-fertilizer amount to characterize the fertilization management of the monitoring sites. Such I_R was 0.54; the result suggested that the ARMOSA model is less robust with regard to climate conditions than the applied N-fertilizer. Anyway, all the calculated I_R were in agreement with values reported by Broose *et al.* (2005) and Confalonieri *et al.* (2010) although they calculated the I_R for other variables such as plant biomass, crop N uptake, LAI, air relative humidity, nitrification rate.

5. CONCLUSIONS

Observed data allowed for the calibration and validation of the ARMOSA model under contrasting conditions of the Lombardy plain, simulating hydrological and nitrogen dynamics. The evaluation outcome confirmed the reliability of the model in predicting (I) crop-related variables, such as above ground biomass, LAI maximum value, harvest index, N uptake, (II) soil water content at different depths, (III) soil NO_3-N content along soil profile, and (IV) N leaching.
Furthermore, the use of ARMOSA shows that N-fertilization was only one of the concurring elements controlling the amount of N leaching. In fact, the crop rotation, together with soil hydrological properties in interaction with water supply, seemed to be relevant factor wich control N leaching. Consequently, optimization of N application in terms of amount have to be defined at very detailed time and space scale, on the basis of cropping system, soil and meteorological conditions.
The ARMOSA model appeared to be a useful tool in evaluating actual agricultural management in terms of productivity and environmental impact in arable land. Future model application could help in defining alternative N fertilization management under different pedoclimatic condition to find a proper combination of production factors able to improve the agroecosystem quality.

ACKNOWLEDGEMENTS

This study was carried out in the project ARMOSA, where soil water and nitrogen dynamics are measured and analyzed under different cropping systems at monitoring sites in arable farms. The project is currently on-going and coordinated by the Department of Agricultural and Environmental Sciences of the University of Milan (DiSAA), the Regional Agency for Agricultural and Forestry Development of Lombardy Region (ERSAF), and the Institute for Mediterranean Agricultural and Forestry Systems - National Research Council of Ercolano (CRN-ISAFOM), Naples.

REFERENCES

Acutis M., Ducco G., Grignani C., 2000. Stochastic use of the LEACHN model to forecast nitrate leaching in different maize cropping systems. European Journal of Agronomy, 13: 191-206.

Acutis M., Brenna S., Pastori M., Basile A., De Mascellis R., Bonfante A., Manna P., Perego A., Fumagalli M., Gusberti D., Velardo M.C., Trevisiol P., Sciaccaluga M., Albani G., Malucelli F., Vingiani S., Orefice N., 2007. “Modellizzazione della dinamica dell’acqua e dell’azoto nei suoli agricoli lombardi - Progetto ARMOSA” - (“Modelling water and nitrate dynamics Nitrogen in Lombardy”) Regione Lombardia quaderno della ricerca n. 65, 124 pp.

Addiscott T.M., Whitmore A.P., 1987. Computer simulation of changes in soil mineral nitrogen and crop nitrogen during autumn, winter and spring. Journal of Agricultural Science, 109: 141-157.

Allen R.G., Pereira L.S., Raes D., Smith. M.,1998. Crop Evapotranspiration: Guidelines for computing crop water requirements. Irrigation and Drainage Paper 56, Food and Agriculture Organization of the United Nations, Rome, 300 p.

Armstrong A.C., Legros J.P., Voltz M., 1996. ACCESS-II: detailed model for crop growth and water conditions. International Agrophysics, 10: 171-184.

Arnold J.G., Srinivasan R., Muttiah R.S., Williams J.R., 1998. Large Area Hydrologic Modeling and Assessment Part I: Model Development. Journal of American Water Resources Association, 34: 73-89.

Arnold J.G., Williams J.R., Nicks A.D., Sammons N.B., 1990. SWRRB: a basin scale simulation model for soil and water resources management. A and M University Press, Texas.

Bechini L., Bocchi S., Maggiore T., Confalonieri R., 2006. Parameterization of a crop growth and development simulation model at sub-model modules level. An example for winter wheat (Triticum aestivum L.). Environmental Modelling Software, 21: 1042-1054.

Bechini L., Castoldi N., 2009. On-farm monitoring of economic and environmental performances of cropping systems: results of a 2-years study at the field scale in Northern Italy. Ecological Indicators, 9: 1096-1113.

Bergstrom L., Johnsson H., Torstensson G., 1991. Simulation of soil-nitrogen dynamics using the SOILN model. Fertilizer Research, 27: 181-188.

Bonfante A., Basile A., Acutis M., De Mascellis R., Manna P., Perego A., Terribile F., 2010. SWAP, CropSyst and MACRO comparison in two contrasting soils cropped with maize in Northern Italy. Agricultural Water Management, 97: 1051-1062.

Broose K., Mertens J., Smolders E., 2005. Toxicity of heavy metals in soil assessed with various soil microbial and plant growth assays: a comparative study. Environmental Toxicology and Chemistry, 24: 634-640.

Burns I.G., 1974. Model for predicting redistribution of salts applied to fallow soils after excess rainfall or evaporation. Journal of Soil Science, 25: 165-178.

Confalonieri R., Bregaglio S., Acutis M., 2010. A proposal of an indicator for quantifying model robustness based on the relationship between variability of errors and of explored conditions. Ecological Modelling, 221: 960-964.

Curiel Yuste J., Janssens A.I., Carrara A., Ceulemans R., 2004. Annual Q10 of soil respiration reflects plant phenological patterns as well as temperature sensitivity. Global Change Biology, 10: 161-169.

Eckersten H., Janssson P.E., Johnsson H., 1996. SOILN model, user’s manual, 3th Ed. Comm. 96:1, Swedish Univ. Agric. Sci., Dpt. of Soil Sciences, Uppsala.

Fernández J.E., Slawinski C., Moreno F., Walczak R.T, Vanclooster M., 2002. Simulating the fate of water in a soil–crop system of a semi-arid Mediterranean area with the WAVE 2.1 and the EURO-ACCESS-II models. Agricultural Water Management, 56: 113-129.

Ferrara R.M., Trevisiol P., Acutis M., Rana G., Richter G.M., Baggaley N., 2010. Topographic impacts on wheat yields under climate change: two contrasted case studies in Europe. Theoretical and Applied Climatology, 99: 53-65.

Fila G., Bellocchi G., Acutis M., Donatelli M., 2003. IRENE: a software to evaluate model performance. European Journal of Agronomy, 18: 369-372.

Fumagalli M., Acutis M., Mazzetto F., Vidotto F., Sali G., Bechini L., 2011. An analysis of agricultural sustainability of cropping systems in arable and dairy farms in an intensively cultivated plain. European Journal of Agronomy, 34. 71-82.

Grignani C., Bassanino M., Sacco D., Zavattaro L., 2003. A nutrient balance for creating a fertilization plan. Rivista di Agronomia, 37: 155-172.

Herrmann A., Taube F., 2004. The range of the critical nitrogen dilution curve for maize (Zea mays L.) can be extended until silage maturity. Agronomy Journal, 96: 1131-1138.

Hutson J.L., 2003. LEACHM. Model description and user's guide. School of Chemistry, Physics and Earth Sciences. The Flinders University of South Australia. GPO Box 2100, Adelaide, SA5001.

Jarvis N.J., 1989. A simple empirical model of root water uptake. Journal of Hydrology, 107: 57-72.

Justes E., Mary B., Meynard J. M., Machet J. M., Thelier-Huch L., 1994. Determination of a critical nitrogen dilution curve for winter wheat crops. Annals of Botany, 74: 397-407.

Kersebaum K.C., 1995. Application of a simple management to simulate water and nitrogen dynamics. Ecological Modelling, 81: 145-156.

Kersebaum K.C., Beblik A.J. 2001. Performance of a nitrogen dynamics model applied to evaluate agricultural management practices. Chapter 17 of 'Modeling carbon and nitrogen dynamics for soil management'. Edited by M.J. Shaffer, Liwang Ma and S. Hansen. Lewis Publischers, pp. 672.

Kersebaum K.C., 2007. Modelling nitrogen dynamics in soil-crop systems with HERMES. Nutrient Cycling in Agroecosystems, 77: 39-52.

Larsbo M., Jarvis N., 2003. MACRO5.0. A model of water flow and solute transport in macroporous soil, Thecnical description 48 Pages, ISBN:91-576-6592-3, 2003.

Larsson M.H., Jarvis N.J., 1999. Evaluation of a dual-porosity model to predict fieldscale solute transport in a macroporous soil. Journal of Hydrology, 215: 153-171.

Loague K., Green R.E., 1991. Statistical and graphical methods for evaluating solute transport models: overview and application. Journal of Contaminant Hydrology, 7: 51-73.

Lord E.I., Shepherd M. A., 1993. Developments in the use of porous ceramic cups for measuring nitrate leaching. Journal of Soil Science, 44: 435-449.

Morari F., Giupponi C., 1997. Effects of four cultivation systems for maize on nitrogen leaching. 2. Model simulation. European Journal of Agronomy, 6: 113-123.

Nash J.E., Sutcliffe J.V., 1970. River flow forecasting through conceptual models part I — A discussion of principles. Journal of Hydrology, 10: 282-290.

Plénet D., Lemaire G., 2000. Relationship between dynamics of nitrogen uptake and dry matter accumulation in maize crops. Determination of critical concentration. Plant Soil 216: 65-82.

Perego A., Basile A., Bonfante A., De Mascellis R., Terribile F., Brenna S., Acutis M., 2012. Nitrate leaching under maize cropping systems in Po Valley (Italy). Agriculture, Ecosystem & Environment, 147: 57-65.

Richter G.M., Acutis M., Trevisiol P., Latiri K., Confalonieri R., 2010. Sensitivity analysis for a complex crop model applied to Durum wheat in the Mediterranean. European Journal of Agronomy, 32: 127-136.

Richter G.M., Rana G., Ferrara R.M., Ventrella D., Acutis M., Trevisiol P., Mayr Th., Baggeley N., Morris, J., Holmes A., Trawick P., Dailey A.G., Robbins P., Simota C., 2006. Stability and mitigation of arable systems in hilly landscapes. EU-QLK-5-CT-2002-013013. Report to the European Commission, Brussels.

Richter G.M., Jaggard K.W., Mitchell R.A.C., 2001. Modelling radiation interception and radiation use efficiency for sugar beet under variable climatic stress. Agricultural and Forest Meteorology, 109: 13-25.

Rocca A., Bellocchi G., Giussani A., Sanna M., Perego A., Fumagalli M., Carozzi M., Chiodini M., Bregaglio S., Confalonieri R., Acutis M., 2013. Correlation between evaluation model indicators. XVI National congress of Agrometeorology. Firenze (Italy), June 4th– 6th, 47-48.

Rozemeijer J.C., van der Velde Y., McLaren R.G., van Geer F.C., Broers H.P., Bierkens M.F.P., 2010. Integrated modeling of groundwater-surface water interactions in a tile-drained agricultural field: The importance of directly measured flow route contributions Water Resources Research, 46, W11537.

Rumbaugh J., Jacobson I., Booch G., 2005. The Unified Modeling Language Reference Manual(2nd Edition) -Addison Wesley2005.

Sinclair T.R., Muchow R.C., Ludlow M.M., Leach G.J., Lawn R.J., Foale M.A., 1987. Field and model analysis of the effect of water deficits on carbon and nitrogen accumulation by soybean, cowpea and Black Gram. Field Crops Research, 17. 121-140.

Stöckle C., Martin S., Campbell G., 1992. A model to assess environmental impact of cropping systems. American Society Agricultural Engineering, Paper No. 92-2041.

Stöckle C.O., Donatelli M., Nelson R., 2003. CropSyst a cropping systems simulation model. European Journal of Agronomy, 18: 289-307.

Van Dam J.C., Feddes R.A., 2000. Numerical simulation of infiltration, evaporation and shallow groundwater levels with the Richards equation: simulation of field scale water flow and bromide transport in a cracked clay soil. Journal of Hydrology, 233: 72-85.

Van Dam J.C., Huygen J., Wesseling J.G., Feddes R.A., Kabat P., van Walsum P., Groenendijk P., van Diepen C.A., 1997. Simulation of water flow, solute transport and plant growth in the Soil-Atmosphere-Plant environment, Theory of SWAP version 2.0, Report 71, Technical Document 45. DLO Winand Staring Centre, Wageningen.

Van der Velde Y., de Rooij G.H., Rozemeijer J.C., van Geer F.C., Broers H.P., 2010. Nitrate response of a lowland catchment: On the relation between stream concentration and travel time distribution dynamics. Water Resources Research, 46, W11534.

Van Heemst H.D.J., 1988. Plant data values required for simple crop growth simulation models: Review and bibliography. Simulation Report CABO-TT nr. 17. Centre for Agrobiological Research (CABO) and Dep. Theoretical Production Ecol., Agricultural University Wageningen, Wageningen, The Netherlands.

Van Keulen H. Wolf J., 1986. Modelling of agricultural production: weather soils and crops. Simulation Monographs. Pudoc, Wageningen, The Netherlands, pp. 479.

Van Keulen H., Penning de Vries F.W.T., Drees E.M., 1982. A summary model for crop growth. In: Penning de Vries, F.W.T., Van Laar, H.H. (Eds.), Simulation of Plant Growth and Crop Production. Simulation Monographs. Pudoc, Wageningen, The Netherlands, pp. 87-98.

Vanclooster M., Viaene P., Diels J., Christiaens K., 1996. WAVE: A mathematical model for simulating water and agrochemicals in the soil and vadose environment, Reference and user's manual, Release 2.1, Institute for Land and Water Management, KU Leuven, Belgium.

Vanclooster M., Viaene P., Diels J., Christianens K., 1994. WAVE: A mathematical model for simulating water and agro-chemicals in the soil and vadose environment. Release 2.0. References and user's manual. Institute for Land and Water Management, Katholieke Universiteit Leuven, Belgium.

Watson C.J., 1986. Preferential uptake of ammonium nitrogen from soil by ryegrass under simulated spring conditions. Journal of Agricultural Science, 107: 171-177.

Wegehenkel M., Mirschel W., 2006. Crop growth, soil water and nitrogen balance simulation on three experimental field plots using the OPUS model- A case study. Ecological Modelling, 190: 116-132.

Micrometeorological methods to measure and model surface energy fluxes of irrigated citrus orchards in a semi-arid environment

Rita Papa[1*], *Simona Consoli*[1]

Abstract: *The object of the research activity was to propose and develop innovative theoretical methods for evaluating mass and energy exchange processes within one of the most relevant crop of the agricultural Sicilian context. The study was conceived as a long monitoring program of micrometeorological features of the study orange orchard at different spatial scales (plant, orchard, farm). Different micrometeorological methods, mainly based on Surface Renewal theory, were studied and tested in order to provide reliable and low cost estimates of sensible heat fluxes within the plant-atmosphere system. Micrometeorological techniques were integrated with* in situ *measurements of transpiration by up-scaled sap flow heat pulse techniques, physiological plant features and microclimatic characteristics of the study area. Derived actual crop evapotranspiration fluxes, by means of the resolution of the energy balance equation opportunely corrected for closure and stomatal resistance, were used to determine crop coefficient values.*
Keywords: *citrus crops, Surface Renewal, Eddy Covariance, aerodynamic methods, irrigation water management.*

Riassunto: *L'obiettivo dello studio è di proporre e sviluppare metodi teorici innovativi per la valutazione dei processi di scambio di massa ed energia con riferimento ad una delle principali colture del contesto agricolo siciliano. Lo studio è stato concepito come un programma di monitoraggio continuo delle caratteristiche micrometeorologiche di un aranceto irriguo a diverse scale spaziali (pianta, frutteto, azienda). Sono stati studiati e testati diversi approcci micrometeorologici, principalmente basati sul metodo denominato Surface Renewal, per ottenere stime affidabili ed economiche dei flussi di calore sensibile scambiati nel sistema pianta-atmosfera. Le tecniche micro meteorologiche adottate nello studio sono state integrate con misure* in situ *di traspirazione ottenute attraverso la tecnica Sap Flow dell'impulso di calore e adeguatamente scalate, attraverso le caratteristiche fisiologiche della pianta e gli aspetti microclimatici dell'area oggetto di studio. I flussi di evapotraspirazione effettiva della coltura, corretti per tener conto degli eventuali errori di chiusura dell'equazione di bilancio energetico e delle stime del termine di resistenza stomatica, sono stati utilizzati per la determinazione dei valori del coefficiente colturale.*
Parole chiave: *colture agrumicole, Surface Renewal, Eddy Covariance, metodi aerodinamici, gestione dell'acqua irrigua.*

1. INTRODUCTION

The understanding of mass (water, carbon dioxide) and energy (solar radiation) exchanges between soil, plants and atmosphere (SPA) *continuum* is a key component for the characterization of the mechanisms controlling hydrology, biota and climate. This understanding requires the availability of reliable methods for the quantification of these mass and energy exchanges encompassing possibly all three major components of the *continuum*. In the applied research addressed to agriculture sector, among these complex mechanisms and exchanges processes, the evapotranspiration (ET) is one of the most important, involving plant activity from root to foliage and the movement of water from soil to air.

The most recognized methods used for ET estimation are usually expensive, difficult to operate and some of them present problems for measurements in heterogeneous vegetation, i.e. the Eddy Covariance method. Therefore, the search for accurate methods to estimate ET fluxes using low-cost, transportable and robust instrumentations is a subject of interest (Castellví *et al.*, 2012; Consoli and Papa, 2012). When the Eddy Covariance (EC) method is used to directly provide measurements of sensible and latent heat flux (or evapotranspiration), a certain un-closure of the energy balance equation can be observed (Consoli and Papa, 2013). Many studies have provided explanations for energy imbalance (Twine *et al.*, 2000; Oncley *et al.*, 2007), including suggestions that there are: (I) sampling errors associated with different measurement source areas for the energy components, (II) systematic bias caused by

* Corresponding author email: rita.papa@gmail.com
[1] Dipartimento di Gestione dei Sistemi Agroalimentari e Ambientali (DiGeSA), University of Catania, Italy.
Received 3 August, accepted 7 September 2013.

calibration, inherent time response and the mounted structures of instruments, (III) neglected energy sinks, (IV) the loss of low and/or high frequency contributions to turbulent flux, and (V) neglected advection of scalars.

Other micrometeorological approaches, such as the Bowen ratio and aerodynamic methods, have a sound theoretical basis and can be accurate as EC method for some surfaces under acceptable conditions.

Micrometeorological measurements and theories identified large organized eddies embedded in turbulent flow, called "coherent structures", as the entities which exchange water vapour, heat and other scalars between the atmosphere and plant communities. Based on these studies, in the year 1991 Paw U and Brunet have proposed the "Surface Renewal" (SR) method for estimating the scalar fluxes. SR theory, in conjunction with the analysis of the observed ramp-like patterns in the scalar traces, provides reliable estimates of the surface flux density of a scalar. The method was tested with air temperature data recorded over various crop canopies, in order to provide estimation of the sensible heat flux. Results of the studies (among other, Snyder *et al.*, 1996; Spano *et al.*, 1997; Consoli *et al.*, 2006; Castellví *et al.*, 2008) have demonstrated good performances of SR in terms of flux density estimations, fitting well with H measurements by EC method.

The theoretical and applied research in the above discussed field of application is very active, and it is aimed at identifying reliable and affordable methods for estimating the mass and energy fluxes exchanges within the SPA *continuum*. Within this context of research, the aim of our study was to investigate, develop and validate integrated approaches to better understand and quantify mass (water) and energy (solar radiation) exchange processes for one of the main tree crop species of the Mediterranean environment. Different micro-meteorological methods, mainly based on Surface Renewal theory, were studied and tested, in order to provide reliable and low cost estimates of sensible heat fluxes within the plant-atmosphere system. Micrometeorological techniques were integrated with *in situ* measurements of transpiration by up-scaled sap flow techniques, physiological plant features (leaf area index, crop surface resistance, etc.), and microclimatic characteristics of the study area to define the evapotranspiration processes and address irrigation water scheduling towards water saving measures.

The results of this study may allow the comprehension of the complex mass and energy exchange processes within the heterogeneous agricultural context of Sicily. This could further facilitate the definition of suitable techniques and methodologies for the rational management of water resources under water scarcity conditions characterizing the area under investigation.

For our better comprehension, the study herein presented is divided into two sections, accordingly to the research program carried out during a two-year monitoring period (2010-2011). The first section was theoretical and mainly based on the improvement of the classic SR method, by introducing a new approach for the calibration factor estimation. The second section was mainly based on determining reliable estimation of ET fluxes by the resolution of the corrected energy balance equation. ET estimates were further corrected to account for the stomatal resistance term, and then compared with the up-scaled transpiration data from the sap flow heat-pulse method.

2. MATERIALS AND METHODS

2.1. Field site description

The experimental activities were carried out in 2010 and 2011 within a citrus orchard of about 120 ha located in Lentini (Eastern Sicily, Lat. 37° 16' N, Long. 14° 53' E), in an area with a Mediterranean semi-arid climate. The experimental field is extended about 25 ha and it is planted with 15÷25-year-old orange trees (*Citrus sinensis* (L.) Osbeck, cv Tarocco Ippolito). The site is flat and the orchard spacing is of 4 m between trunks within rows and 5.5 m between rows. The soil surface is partially covered (10-15%) by natural grass for most of the year. The mean canopy height was 3.75 m. Leaf Area Index (LAI) was estimated using a Licor LAI-2000 (LI-COR, Biosciences) digital analyser and ranged from 3.7 to 4.6 m^2 m^{-2}; the mean LAI was 4.25 m^2 m^{-2}. The foliage is dense from 0.2 m above the ground to the canopy top, and the canopy is nearly continuous along the rows, thus the PAR light interception was 100% in a row and about 50% between rows. For the dominant wind direction (mainly W and NW), the fetch was larger than 550 m. For the other sectors, the minimum fetch was 400 m (SE). The crop was well-watered by drip irrigation supplied every day during the hot months (May÷October), with 4 online labyrinth drippers per plant, spaced at 0.80 m, with a discharge rate of 4 l/h at a pressure of 100 kPa. Soil texture is loam, with 46.85% of sand, 36.25% of silt and 16.90% of clay. The experimental site has ideal conditions for canopy homogeneity, flat slope, size and dominant wind direction, that make the field suitable for micrometeorological techniques application. In summer periods, regional advection for sensible heat fluxes has been reported, i.e. in diurnal periods half-hourly H values were lower than zero (negative) and so opposite in sign to net radiation, R_N (positive).

Numerous instruments were installed at the experimental site in order to derive continuous measurements of energy and mass exchanges in the soil-plant-atmosphere *continuum*; measurements include: weather features, soil water content and sap fluxes. The majority of the equipment is set up on a 10 meter high mast (Fig. 1); low (30 min) and high (10 Hz) frequency data were recorded by four data loggers: a CR3000 Campbell Sci. and three CR1000 Campbell Sci.. Net radiation (R_N) was measured with two net radiometers: one four components (CNR1, Kippen&Zonen) and one integrated (NR-Lite, Kippen&Zonen), deployed above the canopy on a 6 meter mast and facing South.

Soil heat flux density (G) was measured with three soil heat flux plates (HFP01, Campbell Sci.) placed horizontally 0.05 m below the soil surface. Three different measurements of G have been selected: in the trunk row (shaded area), at 1/3 of the distance to the adjacent row, and at 2/3 of the distance to the adjacent row (sunny area). Data from the soil heat flux plates were corrected for heat storage (ΔS) in the soil above the plates, through three probes (TCAV, Campbell Sci.) placed 0.01÷0.04 m (z) below the soil surface. At two heights, 4 and 8 meters, the equipment for Surface Renewal and Eddy Covariance measurements was deployed, so that air temperature, three wind speed components and water vapour were measured. At both levels one fine wire thermocouple (FW3, Campbell Sci., 76.2 µm diameter), one 3-D sonic anemometer (Windmaster Pro, Gill Instruments, at 4 m and CSAT3, Campbell Sci., at 8 m) and one open-path gas analyzer (LI-7500, LI-COR Biosciences) were deployed. Wind components were rotated to force the mean vertical wind speed to zero and to align the horizontal wind speed to the mean streamwise direction; the freely distributed TK2 package (Mauder and Foken, 2004) was used to determine the first and second order statistical moments and fluxes in half-hourly basis following the protocol taken as a reference for comparison described in Mauder *et al.* (2007). Air tempe-


Fig. 1 - Micrometeorological tower (on the left) and HPV probes installed for Sap Flow measurements (on the right).
Fig. 1 - Torre micrometeorologica (a sinistra) e sonde HPV installate per le misure di Sap Flow (a destra).

rature and humidity, wind speed and direction profiles were realized within the orchard with sensors (HMP45C, Vaisala, and A100, Vector Instruments, respectively) installed at 4.5, 6.5, 8.0 and 10.0 meter above the soil surface. Atmospheric pressure (CS106, Campbell Sci.), rainfall (ARG 100, Waterra) and PAR, Photosynthetically Active Radiation (SKP215, Skye Instruments), were measured too. Moreover, to monitor canopy temperature and detect stress conditions onset, four infrared thermometers (IR120, Campbell Sci.) were installed within the orchard, each one pointing at a tree from a cardinal point. Volumetric water content was measured by using the time domain reflectometry theory (TDR) with several probes (CS 616, Campbell Sci.) installed at two different depths below the soil surface.

Heat Pulse Velocity probes (2 in each of the monitored trees, in the North and South faces of the trunk, respectively) 50 mm long, with sensing parts at 5, 15, 25, 45 mm (HP4TC, TranzFlo, NZ) and heaters (HTR5, TranzFlo, NZ) were installed on three orange trees to measure transpiration by the Sap Flow method (Fig. 1).

2.2. An innovative method based on Surface Renewal analysis to estimate sensible heat flux

The SR method is based on the analysis of the observed high frequency scalar (air temperature) traces to extract their mean ramp dimensions, amplitude (A) and time period (τ), allowing to estimate the sensible heat flux (H) as (Paw U *et al.*, 1995)

$$H = \alpha \rho C_p \frac{A}{\tau} z \tag{1}$$

where ρ and C_p are, respectively, the density and specific heat of air at constant pressure, z, is the measurement height of the air temperature trace (i.e. 4 meter in our case) which represents the volume, V, per unit area, S, of the parcel (i.e., z=V/S); the parameter α is included to correct the volume (V) for the unequal heating within the air parcel, and A and τ are, respectively, the mean amplitude and period of the ramp pattern observed in the temperature trace. The Eq. 1 describes the classical SR method, herein referred as SR1. In SR1 α is determined through calibration against the EC measurement of H; in particular, α is the slope of the linear regression equation, between the dependent H from SR1 and the independent H from EC, passing through the origin. A method referred as SR2 was developed to modify α half-hourly estimation:

$$\alpha = \left[\frac{\kappa}{\pi} \frac{\left(z^* - d\right)}{z^2} \tau u_* \phi_h^{-1}(\zeta) \right]^{1/2} \tag{2}$$

where $\kappa = 0.4$ is the Von Kármán constant, d is the zero plane displacement height estimated as a portion of canopy height as $d=0.75h_c$, u_* is the friction velocity which can be estimated as $u_*=0.5\sigma_u$, with σ_u the turbulent standard deviation of the horizontal wind speed measured at the canopy top (Kaimal and Finnigan, 1994), $\varnothing_h\ (\zeta)$ is the flux-gradient stability function and ζ is a stability parameter, $\zeta = (z - d)/L_o$, where L_o is the Obukhov length, $L_o = (u_*^3 / \kappa g(w'T_v'))$ (T_v and g are the air virtual temperature and acceleration due to gravity, respectively, and $w'T_v'$ is the kinematic buoyant sensible heat flux), z^* is the roughness sublayer depth half-hourly estimated as

$$z^* = h_c + \frac{\left(h_c - h_*\right)^2}{\left(h_c - d\right)} \frac{I_u^2}{\left(c_d LAI\right)} \tag{3}$$

where h_* is the height from the ground to the bottom of the canopy, c_d is the leaf drag coefficient, LAI is the leaf area index, and $I_u = (\sigma_u / u)$ is the turbulent intensity, with u the horizontal mean wind speed at the canopy top. The leaf drag coefficient was fit by a trial and error procedure to minimize the root mean square error (RMSE) of H. Both methods (SR1 and SR2) were referred to the height of 4 meters (atmospheric layer close to the canopy top).

Methods SR1 and SR2 were calibrated against the EC measurements of H at 8 meter, level taken as the reference as rule of thumb (twice the canopy height). Linear regression analysis, determination coefficient (R^2) and root mean square error (Rmse) were used to compare H_{SR1} and H_{SR2} versus H_{EC}. Since regression analysis assumes that H_{EC} (the reference) is free of random sampling errors, the coefficient D ($D = \Sigma H_{SR} / \Sigma H_{EC}$) was determined as an integrated evaluation in daily, weekly, monthly, etc. time scales by averaging out errors in the half-hourly estimates (i.e., the bias is (D-1) times the mean of H_{EC}.

2.3. Monitoring evapotranspiration fluxes at different spatial scale

As referred above, the EC technique, allowing for direct measures of H and λE at the orchard scale (i.e. area of footprint), usually leads to an un-closure of the energy balance equation (Consoli and Papa, 2013). To solve this issue, assuming that the measured available energy (R_N-G) is reliable, the Bowen Ratio (BR) method *($\beta = H/\lambda E$)* can be used to proportionally redistribute EC underestimation between sensible (H) and latent (λE) heat fluxes (Twine *et al.*, 2000). So that λE can be estimated as

$$\lambda E = \frac{R_N - G}{1 + \beta} \tag{4}$$

Using the BR-corrected λE fluxes, a crop ET model implementing the Penman-Monteith approach, where the canopy surface resistance was determined from standard microclimatic variables, was applied to determine crop coefficient values (Consoli and Papa, 2013).
Modelled evapotranspiration values were then compared with transpiration rates (T_{SF}) measured at the tree scale by applying the HPV (heat pulse velocity) sap flow technique (Green *et al.*, 2003; Motisi *et al.*, 2012). Transpiration at the tree level was up-scaled to field scale on the basis of the ratio between orchard leaf area index (LAI) and tree LAI. Soil evaporation data were taken into account for ET correction. Values of crop coefficient (K_c) were estimated by the FAO-56 mean K_c approach by using modelled ET data.

3. RESULTS AND DISCUSSION

3.1. Comparison between methods based on SR theory

Three calibration intervals within a nine-month period (from February to October 2010) were chosen for methods SR1 and SR2 to assess α and c_d values (Tab. 1); both unstable and stable atmospheric conditions were evaluated. The α values for method SR1 result quite variable, suggesting the need for continuous calibration through a year. In SR2, the iterative procedure to determine α, leads to stable c_d values, meaning that just few days seem enough for calibrating SR2 (through α) against EC method. The root mean square error (Rmse) values for c_d were smaller than for α under unstable conditions.
Tab. 2 shows the performance of SR1 and SR2 against the EC method in terms of slope (s), intercept (int.), coefficient of determination (R^2), Rmse and coefficient D.
In general, the method SR2 was closer than SR1 to the reference (EC), with smaller Rmse values and higher coefficients of determination. This better performance is also shown in Fig. 2, where H values estimated by SR1 and SR2 were correlated in a linear regression with sensible heat flux measured by EC technique.

Case	α	Rmse	c_d	Rmse
(P: 75÷90)				
Unstable	0.66	61	0.075	37
Stable$^-$	0.32	13	0.2	16
(P: 159÷172)				
Unstable	0.58	75	0.075	62
Stable$^-$	0.21	17	0.2	16
Stable$^+$	0.41	14	0.2	15
(P: 244÷258)				
Unstable	0.76	51	0.075	35
Stable$^-$	0.25	13	0.2	13
Stable$^+$	0.38	9	0.2	11

Tab. 1 - Calibration of α for method SR1 and c_d for method SR2. The Rmse values are in Wm^{-2}; P are the Julian days; + and – denote (R_N-G) positive and negative, respectively.
Tab. 1 - Calibrazione di α per il metodo SR1 e di c_d per il metodo SR2. I valori di Rmse sono espressi in Wm^{-2}; P indica i giorni Giuliani; + e – indicano rispettivamente (R_N-G) positivo e negativo.

3.2. Results on ET rates and Kc values

A certain un-closure of the energy balance equation from EC measurement was observed during the years 2010 and 2011. The percentage of underestimation of H+λE with respect to the available energy was in general not higher than 30%.

	H_{SR1}					H_{SR2}				
Case	s	int.	R^2	Rmse	D	s	int.	R^2	Rmse	D
P: 47÷120										
Unstable	0.92	-11	0.78	56	0.83	0.93	-4	0.87	39	0.90
Stable$^-$	0.42	-8	0.51	19	0.79	0.60	-7	0.72	15	0.90
P: 121÷212										
Unstable	0.90	-15	0.64	73	0.81	1.01	-3	0.77	52	1.00
Stable$^-$	0.19	-11	0.23	20	0.96	0.41	-19	0.29	23	1.60
Stable$^+$	0.20	-10	0.09	21	0.67	0.45	-12	0.13	22	1.05
P: 213÷288										
Unstable	1.11	-24	0.70	56	0.92	1.04	-3	0.79	41	1.01
Stable$^-$	0.27	-12	0.21	16	1.62	0.44	-17	0.21	22	2.15
Stable$^+$	0.58	-5	0.42	12	0.91	0.66	-7	0.50	11	1.09

Tab. 2 - Performance of H_{SR1} and H_{SR2} versus H_{EC} for each three months period. The Rmse and the int. values are in W m^{-2}; P are the Julian days; + and – denote (R_N-G) positive and negative, respectively.
Tab. 2 - Andamento dei valori di H_{SR1} e H_{SR2} rispetto H_{EC} per ciascun periodo di tre mesi. I valori di Rmse e di int. sono espressi in W m^{-2}; P indica i giorni Giuliani; + e – indicano rispettivamente (R_N-G) positivo e negativo.

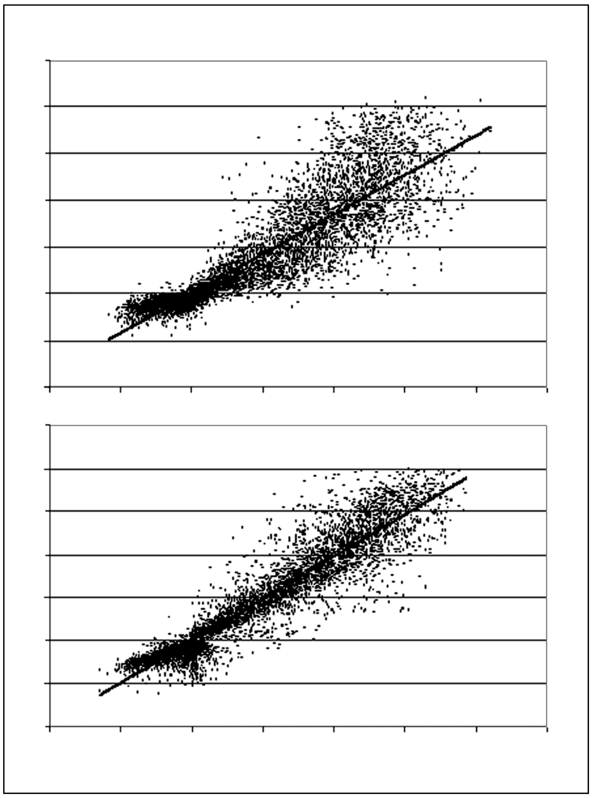

Fig. 2 - H estimates from SR1 and SR2 methods versus H measured by EC.
Fig. 2 - Confronto tra le stime di H ottenute dai metodi SR1 e SR2 e le misure di H da EC.

The BR-based corrections consist on H and λE increase by about 9 and 3%, respectively.
ET values, obtained by dividing the corrected λE by the latent heat of vaporization, were daily aggregated and compared with the up-scaled transpiration (T) data from the HPV Sap Flow method (Fig. 3). The analysis of a mean daily trend in summer months showed a divergence between the two quantities (ET and T) from about 9 a.m. (LST). ET followed the atmospheric water demand, with a peak in the maximum sunny hours, while transpiration fluxes were almost steady with a recovery of flux during the afternoon; the latter can be attributed to tree capacitance. In general, evapotranspiration rates exceeded transpiration of 10%, and this was attributed to the evaporation fraction from the soil.
Fig. 4 reports the crop coefficient calculated daily for the orange orchard under study. Data on K_c from FAO 56 (Allen *et al.*, 1998) refer to constant value of the crop coefficient between 0.45 and 0.65 (it is 0.65 in our experimental conditions), depending on the percentage of crop cover throughout the growth cycle. In this study, K_c varies between 0.20 and 1.10, with a mean value of 0.68.

4. CONCLUSIONS

The analysis of the proposed innovative Surface Renewal method showed that SR2 was superior than SR1, both in term of calibration time and

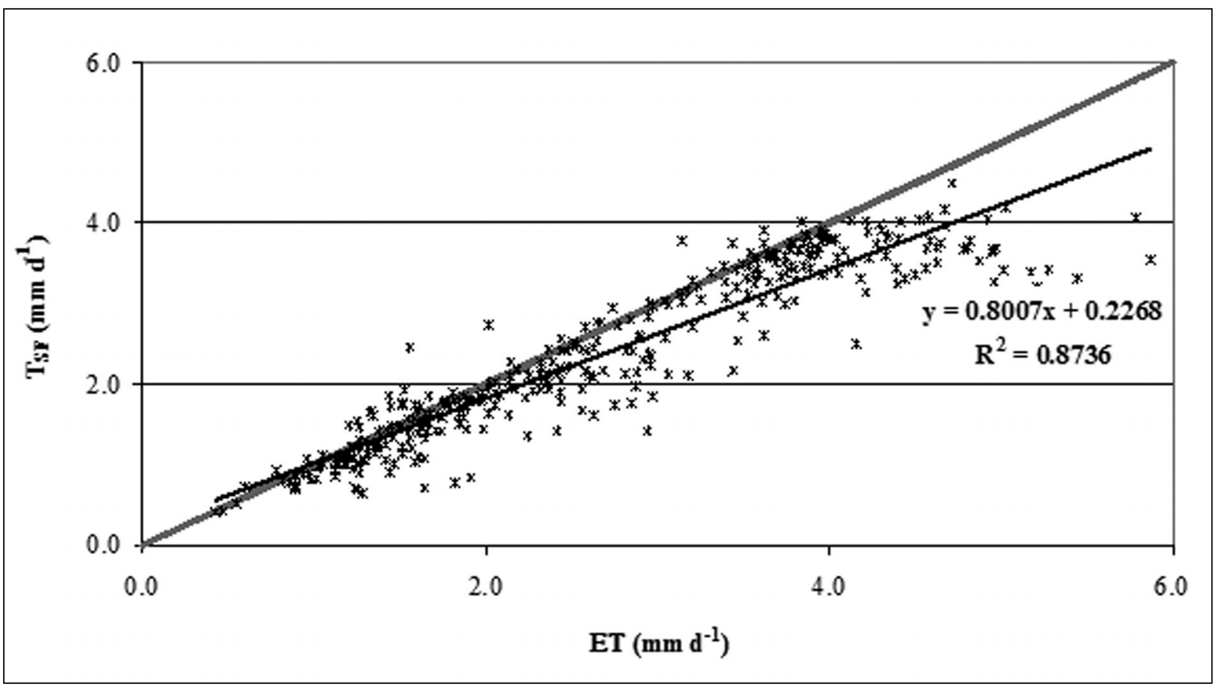

Fig. 3 - Comparison between ET and up-scaled T by Sap Flow.
Fig. 3 - Confronto tra ET e i valori scalati di T da Sap Flow.

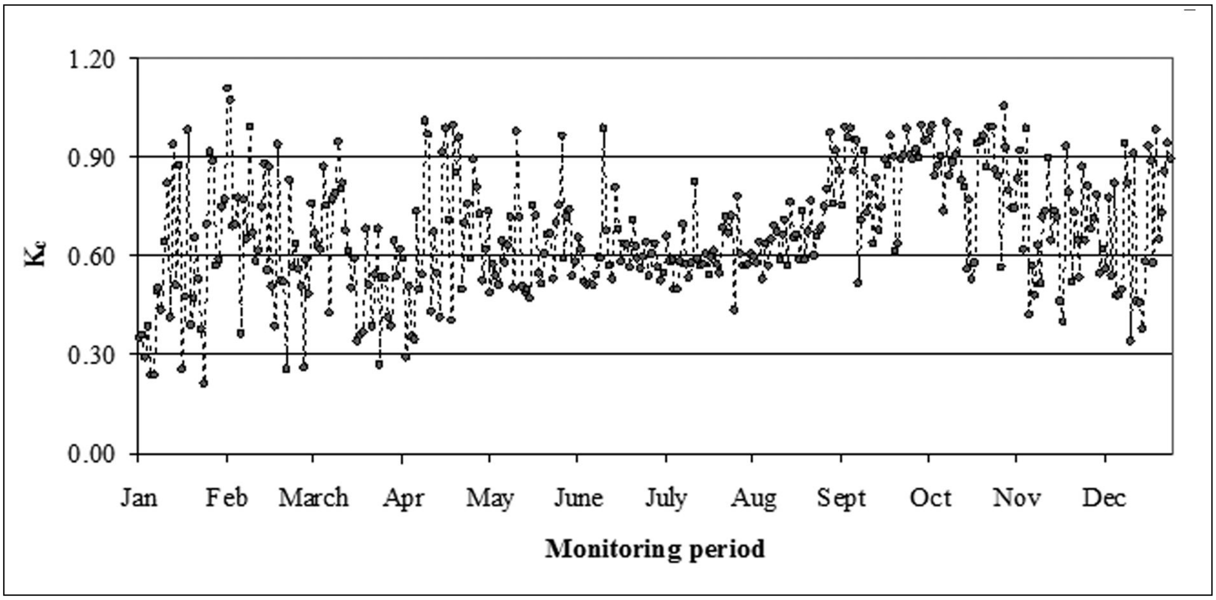

Fig. 4 - Trend of K_c during the monitoring period.
Fig. 4 - Andamento dei valori di K_c durante il periodo in esame.

comparison with EC data. Actually, the suitability of α parameter along the time has been demonstrated to be uncertain, so that application of SR1 method can be onerous. On the contrary, the calibration phase for method SR2 is very limited in time and it depends on weather conditions and canopy characteristics.

On a practical point of view, a more accurate partition of the available energy between sensible and latent heat flux seems very important when adopting Eddy Covariance technique to assess mass and energy exchanges over a crop continuous system. In this direction, the Bowen Ratio approach results appropriate. The comparison between corrected ET data and up-scaled transpiration fluxes allows analyzing the physiological behavior of orange crop under study.

Finally, the efforts involved in this applied research may greatly contribute to enhance knowledge on the exchange processes in the soil-plant-atmosphere *continuum* and may have a significant role for improving irrigation water management within the studied agricultural context.

REFERENCES

Allen R. G., Pereira L. S., Raes D., Smith M., 1998. Crop evapotranspiration, guidelines for computing crop water requirements. Paper No. 56, Rome.

Castellví F., Snyder R. L., Baldocchi D. D., 2008. Surface energy-balance closure over rangeland grass using the eddy covariance method and surface renewal analysis. Agric. Forest Meteorol., 148, 1147-1160.

Castellví F., Consoli S., Papa R. 2012. Sensible heat flux estimates using two different methods based on Surface renewal analysis. A study case over an orange orchard in Sicily. Agric For Meteorol 152:58-64.

Consoli S., O'Connell N., Snyder R. 2006. Estimation of evapotranspiration of different-sized navel-orange tree orchards using energy balance J Irrig Drain Eng 132(1): 2-8.

Consoli S., Papa R. 2012. Estimates of sensible heat flux of heterogeneous canopy crop using different micrometeorological methods. Italian Journal of Agrometeorology Vol. 2 (2), pp.: 37-46 ISSN: 2038-5625.

Consoli S., Papa R. 2013. Corrected surface energy balance to measure and model the evapotranspiration of irrigated orange orchards in semi-arid Mediterranean conditions" Irrigation Science, 31(5): 1159-1171.

Green S. R., Clothier B., Jardine B., 2003. Theory and Practical Application of Heat Pulse to Measure Sap Flow. Agron. J., 95, 1371-1379.

Kaimal J. C., Finnigan J. J., 1994. Atmospheric Boundary Layer Flows: Their Structure and Measurement. Oxford Univ. press., 302 pp.

Mauder M., Foken T., 2004. Documentation and instruction manual of the eddy covariance software package TK2. Universität Bayreuth, Abt.Mikro-

meteorologie, Arbeitsergebnisse, pp. 26-44. http://www.geo.unibayreuth.de/mikrometeorologie/ARBERG.
Mauder M., Oncley S. P., Vogt R., Weidinger T., Ribeiro L., Bernhofer C., Foken T., Kosiek W., De Bruin H. A. R., Liu H., 2007. The energy balance experiment EBEX-2000. Part II. Intercomparison of eddy-covariance sensors and post-field data processing methods. Bound.-Layer Meteorol., 123, doi:10.1007/s10546-006-9139-4.
Motisi A., Consoli S., Rossi F., Minacapilli M., Cammalleri C., Papa R., Rallo G., D'urso G., 2012. Eddy covariance and sap flow measurement of energy and mass exchange of woody crops in a Mediterranean environment. Acta Horticulturae 951, ISHS 2012, pp. 121-127.
Paw U K. T., Brunet Y., 1991. A surface renewal measure of sensible heat flux density. Proc. of the 20th Conference on Agriculture and Forest Meteorology, Salt Lake City, 52-53.
Paw U K. T., Qiu J., Su H.-B., Watanabe T., Brunet Y., 1995. Surface renewal analysis: a new method to obtain scalar fluxes. Agric. Forest Meteorol., 74, 119-137.
Snyder R. L., Spano D., Paw U K. T., 1996. Surface renewal analysis for sensible and latent heat flux density. Bound.-Layer Meteorol., 77, 249-266.
Spano D., Snyder R. L., Duce P., Paw U K. T., 1997. Surface renewal analysis for sensible heat flux density using structure functions. Agric. Forest Meteorol., 86, 259-271.
Twine T. E., Kustas W. P., Norman J. M., Cook D. R., Houser P. R., Meyers T. P., Prueger J. H., Starks P. J., Wesely M. L., 2000. Correcting eddy-covariance flux underestimates over a grassland. Agric. Forest Meteorol., 103, 279-300.

Un semplice apparato sperimentale per la valutazione del corretto funzionamento dei sensori per la misura del flusso di calore nel suolo

Daniele Masseroni[1], Enrico A. Chiaradia[1], Arianna Facchi[1], Claudio Gandolfi[1], Ezio Naldi[1]*

Riassunto: *La misura del flusso di calore attraverso il suolo riveste un ruolo fondamentale nella determinazione degli scambi di energia nei sistemi SVAT (Suolo-Vegetazione-ATmosfera). La misura di tale flusso è generalmente affidata a piastre di piccole dimensioni che sono posizionate in prossimità della superficie del suolo con l'obiettivo di valutare il calore da esso accumulato o ceduto durante il ciclo giornaliero.*

La valutazione del corretto funzionamento delle piastre di flusso e la loro eventuale ricalibrazione è generalmente affidata alle case costruttrici che in alcuni casi si rifiutano di testare sonde che sono già state utilizzate in campo o delle quali sono stati modificati i cablaggi per esigenze sperimentali.

In questo lavoro si descrive un semplice apparato sperimentale, che può essere costruito in qualunque laboratorio, e che permette in primo luogo di verificare se i sensori di flusso funzionino correttamente, valutando gli andamenti del flusso di calore misurati in risposta a differenti gradienti termici imposti alle due facce della piastra. In secondo luogo, l'apparato sperimentale consente di verificare se le costanti di sensitività fornite all'acquisto dalla casa madre (differenti per ciascun sensore)siano corrette , confrontando gli andamenti dei flussi di calore misurati dalla piastra con quello ottenuto applicando la legge di Fourier, note le temperature applicate alle facce e la conducibilità termica della piastra stessa.L'utilizzo di materiali semplici e facilmente reperibili in qualunque laboratorio rendono questo strumento facilmente riproducibile, e i risultati mostrati dimostrano che l'apparato sperimentale consente di raggiungere gli obiettivi prefissati.

Parole chiave: *piastre di flusso, gradiente termico, flusso di calore nel suolo.*

Abstract: *Soil heat flux plays an important role into the SVAT (Soil-Vegetation-ATmosphere) energy exchanges. Soil heat flux is usually measured by small plates located close to the soil surface.*

The evaluation of the correct functioning of the soil heat flux plates is generally performed by the manufacturers that in some cases refuse to test probes that have already been used in the field or which have been modified for specific experimental needs.

In this paper we describe a simple apparatus that can be built in any laboratory and allows in the first place to check whether the heat flux sensors are working properly, considering the pattern of the heat flux measured in response to different thermal gradients imposed on the two sides of the plate. Secondly, the experimental apparatus allows to verify whether the sensitivity constants provided to the manufacturers (different for each sensor)are corrected , comparing the measured heat flux pattern with that obtained by applying the Fourier law, knowing the temperatures applied to the two plate faces and the thermal conductivity of the plate.

The use of simple materials readily available in any laboratory make this apparatus easily reproducible, and the results show that experimental setup allows the achievement of the experimental objectives.

Keywords: *heat flux plates, temperature gradient, soil heat flux.*

1. INTRODUZIONE

Il flusso di calore attraverso il suolo è una componente fondamentale del bilancio energetico nel sistema suolo-vegetazione-atmosfera. Generalmente di difficile determinazione, tale flusso viene di norma misurato attraverso piastre di ceramica/plastica con diametri dell'ordine dei 10 cm e spessore 5 mm. Tipicamente in molte sperimentazioni vengono utilizzate piastre prodotte dalla Hukseflux (NL) (Masseroni *et al.* 2011), che all'interno sono costituite da una termopila che è in grado di percepire le differenze di temperatura tra la faccia superiore ed inferiore della piastra. Il segnale elettrico in output risulta proporzionale al gradiente termico percepito dal sensore ed il flusso viene ottenuto conoscendo la conducibilità termica del materiale plastico-ceramico (HFP01 e HFP03 User Manual, Hukseflux).

Nonostante il grande proliferare di siti sperimentali agro-meteorologici sia nel contesto nazionale

* Corresponding author e-mail: daniele.masseroni@unimi.it

[1] Dipartimento di Scienze Agrarie e Ambientali – Produzione, Territorio e Agroenergia, Università degli Studi di Milano, Italy.

Received 29 June 2013, accepted 11 July 2013.

che internazionale, in letteratura non sono presenti molti lavori che riportano risultati di calibrazioni o valutazioni di corretto funzionamento di questi sensori (Biscoe *et al.* 1997). Generalmente i test che vengono effettuati possono essere classificati in due grandi categorie: calibrazioni di laboratorio (van Loon *et al.* 1998) o in situ (Douglas and Baker 2003). Mentre i test in ambiente controllato possono essere gestiti con maggiore sicurezza, la calibrazione in situ risente di fattori connessi all'evapotraspirazione, alla variazione della radiazione solare e all'umidità del suolo che alterano la conducibilità termica del mezzo materiale e che difficilmente possono essere indagati separatamente. Tuttavia, il grosso problema che accomuna entrambi i test, è la necessità di conoscere la conducibilità termica del suolo utilizzato durante l'esperimento. Tale proprietà dipende dall'umidità, dalla temperatura e dalle caratteristiche geotecniche del suolo stesso (Woodward and Sheehy 1983).

In questo lavoro si presenta un apparato sperimentale che permette di testare le piastre di flusso della tipologia Hukseflux HFP01 prescindendo dalla conoscenza della conducibilità termica del suolo ma conoscendo solamente il valore di conducibilità della piastra stessa, facilmente reperibile dal manuale d'uso della stessa. L'esperimento si basa sulla creazione e il mantenimento di un gradiente termico tra le facce della piastra testata. Attraverso la legge di Fourier, note le temperature applicate alle facce e la conducibilità termica della piastra, si calcola il flusso di calore che teoricamente attraversa il sensore e successivamente lo si paragona con quello misurato dalla sonda. Attraverso l'utilizzo di questo apparato è anche possibile testare contemporaneamente più piastre di flusso poste in serie tra loro, sfruttando il principio di conservazione dell'energia termica che attraversa in egual misura tutte le piastre sovrapposte.

2. MATERIALI E METODI

In questo esperimento sono state testate contemporaneamente due piastre di flusso Hukseflux HFP01 (Campbell Scientific) che, insieme a due termistori 107L (Campbell Scientific), sono state collegate direttamente ad un DataLogger CR1000 (Campbell Scientific). Le piastre sono identificate mediante un numero di serie: 6753 per il primo sensore e 1394 per il secondo, e hanno rispettivamente una costante di sensitività pari a 61.7 e 61.9 (indicata sul certificato di taratura). Questi sensori sono stati acquistati in due anni differenti, il 6753 nel 2011 e il 1394 nel 2005, non sono mai stati mandati alla casa madre per una verifica di funzionamento e hanno operato sul campo entrambi fin dalla data del loro acquisto. L'obiettivo di questo esperimento, oltre a verificare il buon funzionamento dell'apparato sperimentale, mira anche a mostrare se questa tipologia di sensori risulti essere duratura nel tempo resistendo alle sollecitazioni fisico/meccaniche che si verificano nel corso di intere campagne sperimentali.

La struttura base dell'apparato sperimentale è costituita da due spesse lastre di alluminio di lato 20/30 cm e spesse 2 cm circa che, grazie alla loro alta conducibilità termica, si scaldano uniformemente e in tempi rapidi. In particolar modo solo la piastra superiore viene riscaldata utilizzando la testa di un saldatore a stagno di 60W di potenza che, attraverso una modifica, è stato connesso al DataLogger. Tramite quest'ultimo, e grazie all'ausilio di un relè, il saldatore viene spento automaticamente una volta raggiunto il gradiente di temperatura voluto. La temperatura della lastra inferiore tende a rimanere costante e pari a quella dell'ambiente di laboratorio. Le temperature delle lastre di alluminio vengono monitorate con continuità attraverso due termistori agganciati rispettivamente sulle superfici delle lastre e opportunamente isolate con del materiale termoresistente in modo tale che non risentano dell'influenza di variazioni di temperatura esterne a quelle delle lastre stesse (Fig. 1).

Le piastre di flusso che devono essere testate, sono state posizionate orizzontalmente l'una sopra l'altra tra le due lastre di alluminio e circondate da materiale termoisolante in modo tale che il calore tra una lastra e l'altra si trasferisca solo per conduzione attraverso le piastre (Fig. 2A). Tutto l'apparato è stato saldamente tenuto insieme attraverso l'utilizzo di morsetti in ferro che impediscono gli spostamenti di ciascuna delle parti e in Fig. 2B è mostrato l'apparato completo.

L'apparato sperimentale di Fig. 2B, seppur di notevole semplicità costruttiva, permette di valutare contemporaneamente il comportamento di due o più piastre di flusso. Questo risulta di notevole interesse pratico soprattutto nella valutazione della risposta delle sonde a differenti sollecitazioni di gradienti termici variabili nel tempo. Se le sonde funzionano correttamente, infatti, ci si aspetta di ottenere curve di flusso con andamenti sovrapponibili, a meno di brevi ritardi dovuti al transiente di tempo necessario al passaggio del flusso di calore attraverso le piastre. All'equilibrio le curve di flusso delle diverse sonde dovrebbero essere sovrapposte l'una all'altra e coincidenti con quella

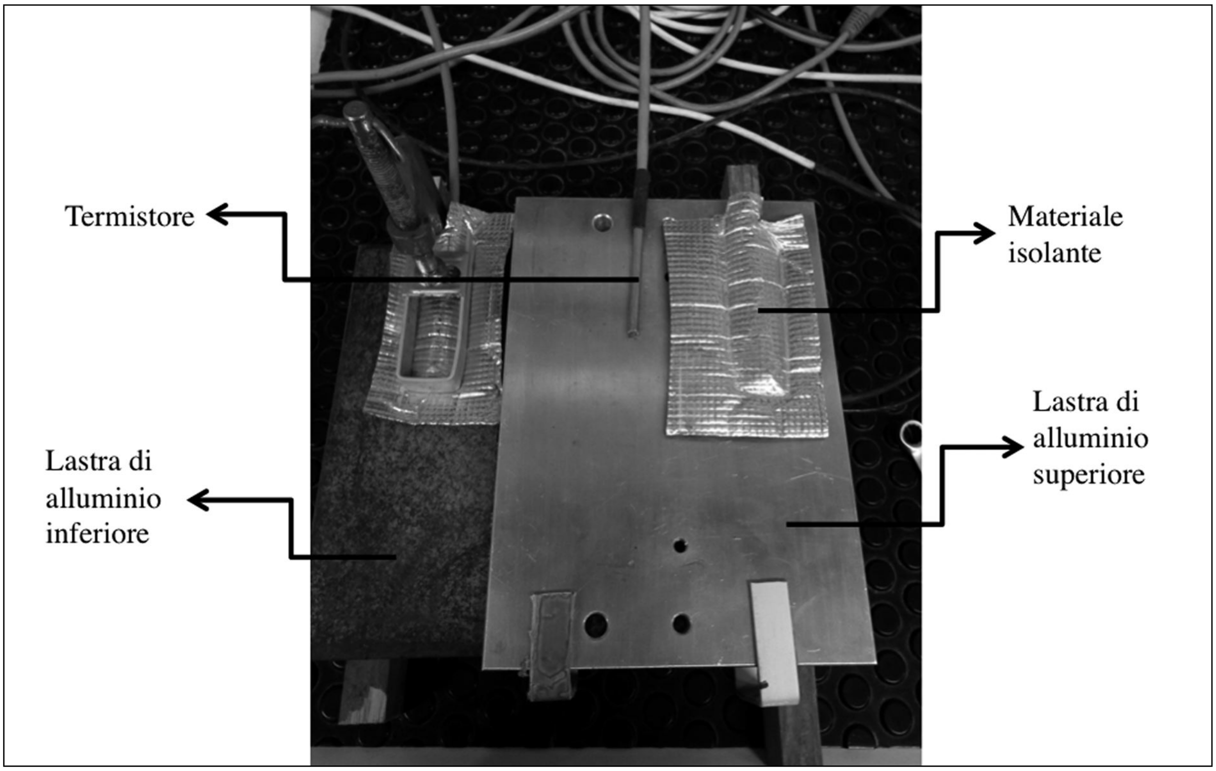

Fig. 1 - Porzione dell'apparato sperimentale. Lastre di alluminio e termistori.
Fig. 1 - Experimental apparatus. Aluminum sheets and thermistors.

di riferimento calcolata a tramite la legge di Fourier, a partire dalla differenza di temperatura misurata dai termistori e dalla conducibilità termica delle piastre. Attraverso l'utilizzo di un apparato così costruito, è possibile allo stesso tempo generare gradienti termici molto maggiori rispetto a quelli che si verificherebbero in natura sotto la superficie del terreno, portando le piastre anche in condizioni limite e valutandone il comportamento sul lungo periodo. I cicli termici prodotti con l'ac-

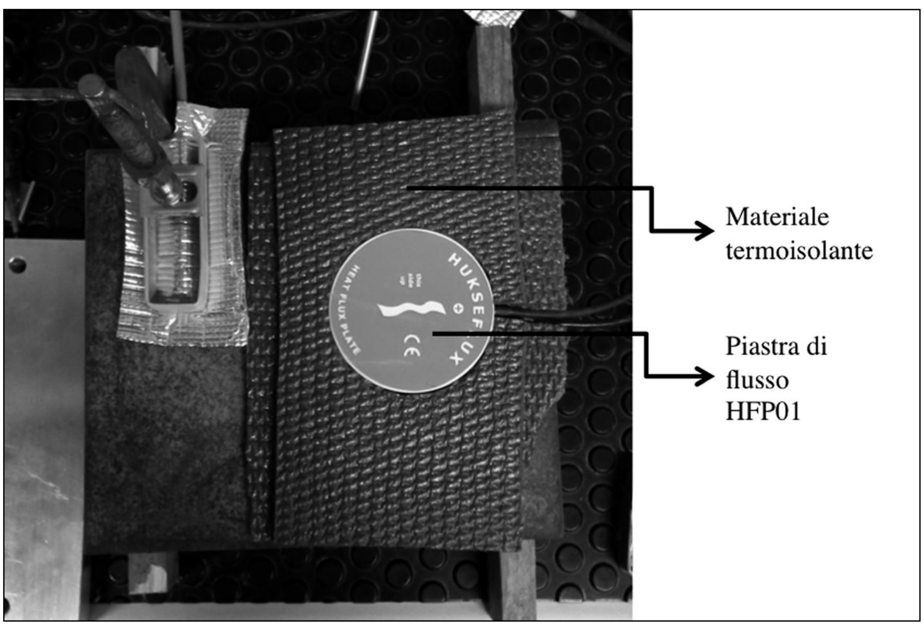

Fig. 2.A - Posizionamento delle piastre di flusso Hukseflux all'interno dell'apparato sperimentale.
Fig. 2.A - Heat flux plates position in the experimental apparatus. B.

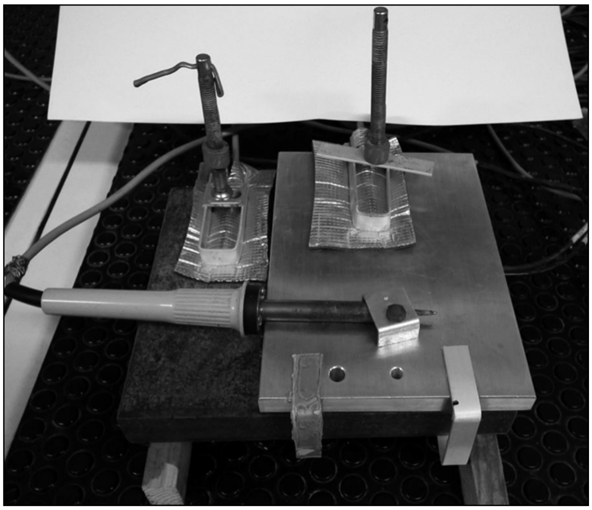

Fig. 2.B - Apparato completo.
Fig. 2.B - Experimental apparatus with all the components.

censione e lo spegnimento del riscaldatore permettono così di coprire un ampio intervallo di gradienti termici e di conseguenza di valutare se la sensitività di ciascuna piastra di flusso necessita di una ricalibrazione. L'assenza dell'utilizzo di suolo rispetto alle esperienze di laboratorio affrontate da van Loon *et al.* (1998) permette di eliminare il problema connesso alla determinazione della sua conducibilità termica, necessitando solamente di quella delle piastre (0.8 W m^{-1} K^{-1} costante per ciascun sensore), ricavata nelle specifiche di costruzione delle sonde.

3. RISULTATI E DISCUSSIONI

L'esperimento è consistito nel confrontare i flussi di calore delle due piastre con quello ottenuto dalla legge di Fourier. I flussi delle piastre sono dati dal rapporto tra il voltaggio in output dai sensori e la costante di sensitività di ciascuno di essi. Il flusso di calore dalla legge di Fourier, invece, è stato ricavato a partire dal gradiente termico generato dalle lastre di alluminio moltiplicato per la conducibilità termica delle piastre di flusso.

In Fig. 3 sono rappresentati i flussi di calore misurati da entrambe le piastre, confrontati con quello ricavato implementando la legge di Fourier. Sul secondo asse delle ordinate è inoltre rappresentato l'andamento delle temperature delle lastre di alluminio. La temperatura della lastra inferiore rimane pressoché costante, con un graduale incremento nel corso dell'esperimento da 20 a 23°C circa, mentre quella superiore varia, a conseguenza dei continui cicli di riscaldamento e raffreddamento, tra 18 e 37 °C. Si è inoltre operato in modo da generare un gradiente termico negativo (dopo circa 30 minuti dall'inizio dell'esperimento, come si evince dalla figura), raffreddando la lastra superiore con del ghiaccio. A conseguenza di questo raffreddamento i flussi di calore misurati dalle piastre hanno cambiato segno e sono passati da positivi a negativi.

Dagli andamenti dei flussi riportati in Fig. 3 si osserva un leggero ritardo dei picchi e delle gole della curva rappresentante il flusso di calore ricavato dalla legge di Fourier rispetto a quello delle

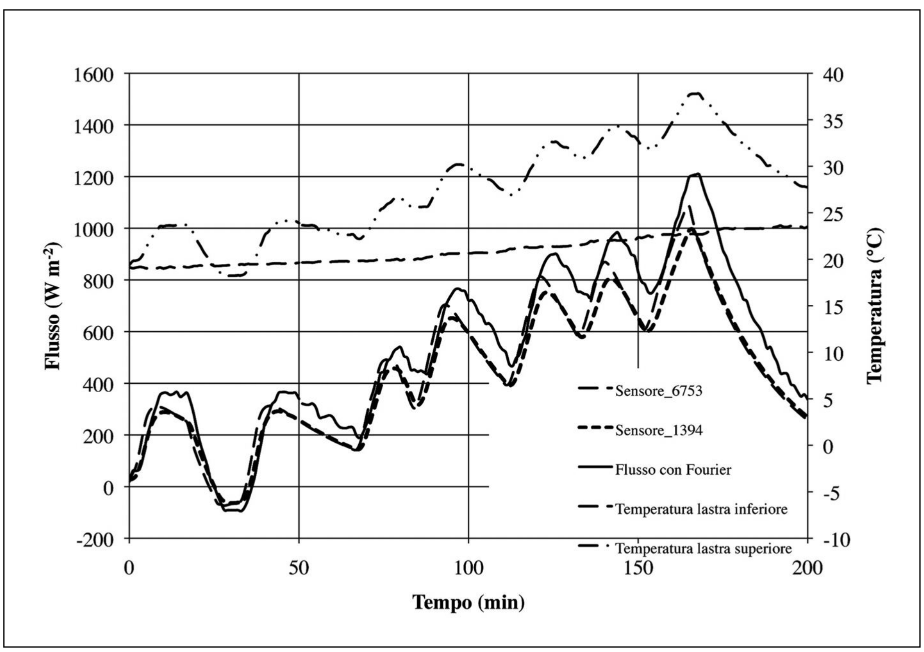

Fig. 3 - Andamento dei flussi di calore delle piastre rispetto a quello calcolato dalla legge di Fourier durante l'esperimento di laboratorio.
Fig. 3 - Comparison between heat fluxes measured by plates and Fourier law.

piastre di flusso. Questo può essere imputabile alla diversa natura dei sensori utilizzati nell'esperimento (i.e., termistori e piastre di flusso) che hanno tempi di risposta differenti alle diverse sollecitazioni. Infatti i termistori essendo dei resistori che per loro natura variano la loro resistenza in funzione della temperatura di sollecitazione, rispondono con tempistiche differenti rispetto alle termopile che invece sono di base costituite da termocoppie.

Come si evince dalla Fig. 3 il comportamento di entrambe le piastre di flusso è pressoché coincidente. Entrambe rispondo all'unisono alle sollecitazioni dei gradienti termici e solo per elevati valori di flusso (> 600 W m^{-2}), difficilmente verificabili in siti sperimentali, le risposte dei due sensori differiscono tra loro. Il fatto che sensori acquistati rispettivamente nel 2005 e nel 2011 e da allora sempre utilizzati per misure in condizioni di pieno campo forniscano tali risultati, garantisce il fatto che tali strumenti siano robusti e che la deriva strumentale sia contenuta. L'andamento dei flussi misurati dalle piastre sottostima leggermente quello calcolato dalla legge di Fourier, discostandosi soprattutto nel caso di elevati gradienti termici. Questo ritardo può essere conseguenza della dinamica di stimolazione delle piastre che risulta essere più rapida di quella naturale con la conseguente diversificazione dei tempi di risposta della termopila. Inoltre i complessi meccanismi di propagazione del calore all'interno delle piastre di alluminio potrebbero essere la causa della non perfetta uniformità della temperatura delle stesse generando delle differenze tra i flussi misurati e quelli modellati dalla legge di Fourier. Tuttavia, calcolando l'errore relativo medio percentuale commesso dai sensori rispetto al flusso ricavato dalla legge di Fourier per l'intera durata dell'esperimento, si è ottenuto che per il sensore 6753 e il 1394 lo scostamento dal valore teorico è dell'ordine del -20% e del -24% rispettivamente.

Analizzando gli errori per gradienti di temperatura tali da produrre flussi nell'intervallo di 0 e 400 W m^{-2} (valori tipici riscontrabili nei siti sperimentali agro-meteorologici), lo scostamento del flusso misurato rispetto a quello ottenuto dalla legge di Fourier scende a valori di circa il -15% e -20%, rispettivamente per la sonda 6753 e 1394.

L'attendibilità delle misure di flusso condotte dalle due piastre è stata infine valutata per differenti intervalli di aggregazione temporale dei dati. Infatti, le normali acquisizioni in situ sono generalmente mediate su scale di mezz'ora mentre in questa esperienza i dati sono stati registrati ogni minuto. Applicando differenti scale di aggregazione temporale pari a 1, 5, 10, 20 e 30 minuti si è notato un leggero decremento dell'errore relativo medio percentuale che diminuisce del 7%, rispetto ai valori precedentemente riscontrati, per tempi di aggregazione pari a 30 minuti.

4. LIMITAZIONI

Alcuni limiti dell'apparato sperimentale riguardano soprattutto la difficoltà di mantenere piccoli gradienti termici tra le piastre per lunghi periodi di tempo. È infatti opportuno il più possibile evitare il trasferimento di calore da quella superiore (riscaldata) a quella inferiore (non riscaldata). Per fare ciò il materiale isolante interposto tra le piastre deve essere accuratamente posizionato in modo tale che solo le facce delle piastre di flusso siano a contatto con quelle delle lastre di alluminio. Inoltre è piuttosto complesso governare l'inerzia termica della piastra di alluminio durante le fasi di riscaldamento. È perciò consigliato accendere e spegnere frequentemente in riscaldatore (con intervalli dell'ordine dei 20-30 secondi), in modo tale da procedere gradualmente al riscaldamento della piastra di alluminio superiore fino alla temperatura desiderata.

Per testare la risposta a gradienti negativi, si può procedere con il raffreddamento della piastra superiore fino ad una temperatura più bassa di quella della lastra di alluminio di base, oppure si può procedere inserendo al rovescio le piastre di flusso all'interno dell'apparato sperimentale. A parità di gradienti termici si dovranno così ottenere flussi di calore uguali ma con segno negativo.

5. CONCLUSIONI

Nella nota è stato descritto un semplice apparato sperimentale atto a verificare contemporaneamente il corretto funzionamento di una o più piastre di flusso della tipologia Hukseflux HFP01. L'apparato è costituito da due lastre di alluminio sovrapposte, due termistori, un Datalogger, e una fonte di calore, ottenuta utilizzando la testa di un saldatore a stagno, modificato in modo da poter essere pilotato dal DataLogger. L'apparato è quindi realizzabile con materiali di basso costo e richiede strumentazione facilmente reperibile.

Le piastre di flusso sono disposte una sopra l'altra e collocate tra le due lastre di alluminio, circondandole con materiale termoisolante, che separa l'intera superficie residua delle lastre. Con l'ausilio dei termistori è possibile calcolare il valore della differenza di temperatura tra le lastre, a seguito di sollecitazioni termiche imposte in modo control-

lato alla lastra superiore tramite il saldatore a stagno. Applicando la legge di Fourier si ottiene quindi il valore di riferimento del flusso di calore scambiato tra le due lastre, sulla base del quale è possibile verificare le misure fornite dalle piastre di flusso confutare i coefficienti di sensitività.
I risultati ottenuti dimostrano l'efficacia dell'apparato sperimentale, che può essere facilmente riprodotto e si presta ad ulteriori sviluppi per condurre prove sperimentali più complesse.

BIBLIOGRAFIA

Biscoe P., Saffell R., & Smith P. (1977). An apparatus for calibrating soil heat flux plates. *Agricultural and Forest Meteorology*, 18: 49-54.

Cobos D., & Baker J. (2003). In situ measurement of soil heat flux with gradient method. *Vadose Zone Journal*, 2: 589-594.

Masseroni D., Ravazzani G., Corbari C., & Mancini M. (2011). Correlazione tra le dimensioni del footprint e le variabili esogene misurate da stazioni eddy covariance in Pianura Padana, Italia. *Italian Journal of Agrometeorology*, 1:1-12.

van Loon W., Bastings H., & Moors E. (1998). Calibration of soil heat flux sensors. *Agricultural and Forest Meteorology*, 92: 1-8.

Woodward F., & Sheehy J. (1983). *Principles and measurements in environmental biology.* London, UK: Butterworths 263 pp.